ARL-TR-9000 ● JULY 2020

DEVCOM ARMY RESEARCH LABORATORY

Comprehensive Assessment of Overall Quality of Several Specimens from an As-Cast FeMnAl Steel Alloy Ingot via X-ray Computed Tomography

by William H Green, Bryan A Cheeseman, Daniel M Field, and Krista R Limmer

NOTICES

Disclaimers

The findings in this report are not to be construed as an official Department of the Army position unless so designated by other authorized documents.

Citation of manufacturer's or trade names does not constitute an official endorsement or approval of the use thereof.

Destroy this report when it is no longer needed. Do not return it to the originator.

ARL-TR-9000 ● JULY 2020

Comprehensive Assessment of Overall Quality of Several Specimens from an As-Cast FeMnAl Steel Alloy Ingot via X-ray Computed Tomography

William H Green, Bryan A Cheeseman, Daniel M Field, and Krista R Limmer
Weapons and Materials Research Directorate, CCDC Army Research Laboratory

REPORT DOCUMENTATION PAGE

Form Approved
OMB No. 0704-0188

1. REPORT DATE *(DD-MM-YYYY)*	2. REPORT TYPE	3. DATES COVERED (From - To)
July 2020	Technical Report	1 August 2018–31 January 2020

4. TITLE AND SUBTITLE
Comprehensive Assessment of Overall Quality of Several Specimens from an As-Cast FeMnAl Steel Alloy Ingot via X-ray Computed Tomography

5a. CONTRACT NUMBER

5b. GRANT NUMBER

5c. PROGRAM ELEMENT NUMBER

6. AUTHOR(S)
William H Green, Bryan A Cheeseman, Daniel M Field, and Krista R Limmer

5d. PROJECT NUMBER

5e. TASK NUMBER

5f. WORK UNIT NUMBER

7. PERFORMING ORGANIZATION NAME(S) AND ADDRESS(ES)
CCDC Army Research Laboratory
ATTN: FCDD-RLW-MB
Aberdeen Proving Ground, MD 21005

8. PERFORMING ORGANIZATION REPORT NUMBER
ARL-TR-9000

9. SPONSORING/MONITORING AGENCY NAME(S) AND ADDRESS(ES)

10. SPONSOR/MONITOR'S ACRONYM(S)

11. SPONSOR/MONITOR'S REPORT NUMBER(S)

12. DISTRIBUTION/AVAILABILITY STATEMENT
Approved for public release; distribution is unlimited.

13. SUPPLEMENTARY NOTES
ORCID ID(s): Krista R Limmer, 0000-0003-4775-5876; William H Green, 0000-0001-8772-3946

14. ABSTRACT
The X-ray computed tomography (XCT) technique is a widely applicable and powerful nondestructive inspection modality to evaluate and analyze geometrical and physical characteristics of materials, especially internal structures and features. XCT is applicable to metals, ceramics, plastics, and polymer and mixed composites, as well as components and materiel. The US Army Combat Capabilities Development Command Army Research Laboratory and its partners are currently investigating the use of cast iron-manganese-aluminum (FeMnAl) steel alloy material in support of weight reduction initiatives in Army development programs. Steel alloy FeMnAl has been identified as a key enabling material technology to reduce the weight in ground combat vehicle systems. A set of FeMnAl blocks, each approximately 50.8 mm (2 inches) thick by 76.2 mm (3 inches) wide by 76.2 mm (3 inches) long, which had been sectioned from an industrially cast ingot (~12,000 lb), were individually scanned by XCT using a conventional 450-kV X-ray source and a solid-state flat panel detector. Due mainly to the thickness of the blocks, as well as a desire to keep geometric unsharpness relatively small, which affected overall scan geometry (setup), the scans had a very low response at the detector through the FeMnAl blocks. With the calibrated detector response through air (i.e., around a block) at 85%–90%, the response through the block was only 5%–10%. This report covers the XCT scanning parameters and overall protocol used to mitigate the very low intensity throughput and achieve acceptable scan image results; the overall quality of the FeMnAl blocks and comparisons of the block sets to one another is also discussed.

15. SUBJECT TERMS
porosity/voids, FeMnAl, X-ray computed tomography, image noise, qualitative

16. SECURITY CLASSIFICATION OF:			17. LIMITATION OF ABSTRACT	18. NUMBER OF PAGES	19a. NAME OF RESPONSIBLE PERSON
a. REPORT	b. ABSTRACT	c. THIS PAGE			William H Green
Unclassified	Unclassified	Unclassified	UU	69	19b. TELEPHONE NUMBER (Include area code) (410) 306-0817

Contents

List of Figures

List of Tables

1. Introduction and Background

The X-ray computed tomography (XCT) technique is a widely applicable and powerful nondestructive inspection modality to evaluate and analyze geometrical and physical characteristics of materials, especially internal structures and features. XCT is applicable to metals, ceramics, plastics, and polymer and mixed composites, as well as components, assemblies, and materiel. The principal advantage of XCT is that it provides densitometric (that is, radiological density and geometry) images of thin cross sections through an object in a noninvasive manner. Because of the absence of structural superimposition, images are much easier to interpret than conventional radiological images.[1–4]

The US Army Combat Capabilities Development Command (CCDC) Army Research Laboratory (ARL) and its partners are currently investigating the use of cast iron-manganese-aluminum (FeMnAl) steel alloy material in support of weight reduction initiatives in Army development programs. Steel alloy FeMnAl has been identified as a key enabling material technology to reduce the weight in ground combat vehicle systems. A large industrial FeMnAl alloy ingot several meters (feet) long, 1.32 m (52 inches) wide, and 0.305 m (12 inches) thick with a nominal chemistry of Fe-30Mn-9Al-0.8Si-1C-0.5Mo was produced by electric arc furnace melting in a 40T heat and subsequent casting using a bottom pour method, after which a normalization heat treatment was performed. XCT scanning of several specimens sectioned from three different solidification areas of the ingot determined the internal mesoscale structure of these areas and identified a number of significant individual features. The solidification areas included a central region in the middle (thickness) of the ingot and regions just inside the outside edges of the ingot along the 1.32-m width. In this report the locations and organization of the sectioned specimens will be given. The XCT scanning parameters and overall protocol used to mitigate the very low-intensity throughput and achieve acceptable scan image results will be discussed, as well as scan results of interior structure and features of each solidification area. Physical features of each set of blocks are compared and contrasted, and a comprehensive overall assessment of the blocks is given.

2. Preparation of FeMnAl Specimens

After the normalization treatment, a 76.2-mm (3-inch)-wide slice from just below the hot top of the ingot was removed for analysis. A water jet method was used to remove fourteen 50.8- × 76.2- × 76.2-mm (2- × 3- × 3-inch) blocks from the ingot slice according to the schematic in Fig. 1, in which the width of the ingot is left-to-

right, the thickness direction is vertical, and the 76.2-mm (3-inch) slice direction is into the page. The solidification direction is from the outside toward the inside, and the filling or casting direction is coming out of the page. Six blocks were sectioned from the middle interior of the ingot slice, labeled C1 to C6, as shown in Fig. 1. Four blocks each were sectioned from two outside regions on either side of the middle interior region to be representative of possible solidification effects in the same area, labeled A1 to A4 and B1 to B4, as shown in Fig. 1.

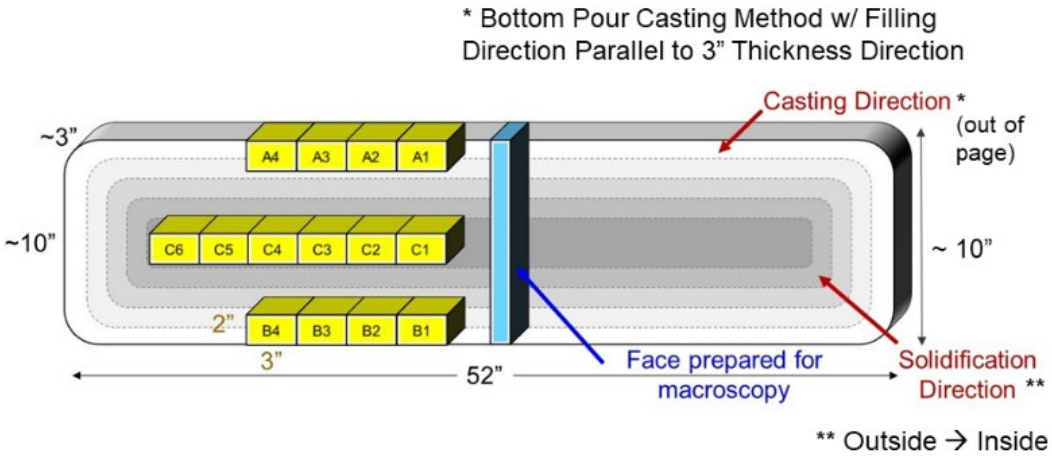

Fig. 1 Schematic of specimen blocks sectioning

3. XCT Scanning Procedures

Given that the approximately 76.2- × 76.2-mm (3- × 3-inch) steel alloy FeMnAl blocks were 50.8 mm (2 inches) thick, the attenuation of 450-keV maximum energy polychromatic Bremsstrahlung X-rays was high. Although not generally explicitly stated in standards on XCT practice,[1,5] a general rule of thumb sometimes used in industrial XCT is to set up the scan procedure such that approximately 50% of the initial X-ray intensity from the X-ray source is attenuated by the object of interest. The purpose of this approach is to have a balance between image contrast and intensity, or signal, at the detector, and hence signal-to-noise ratio (S/N), in the XCT scans. XCT scans can still be performed with attenuation factors significantly below or above 50% with resultant effects of loss of contrast or loss of detector signal and possibly decrease in S/N. However, XCT images generated from these types of scans can still show pertinent physical information and features and provide acceptable physical data about a specimen.

Figure 2 shows a 2-D X-ray projection image through the 50.8-mm (2-inch) thickness of one of the FeMnAl blocks using the X-ray technique (tube energy and current) of the XCT scan method, the parameters of which are given in Table 1.

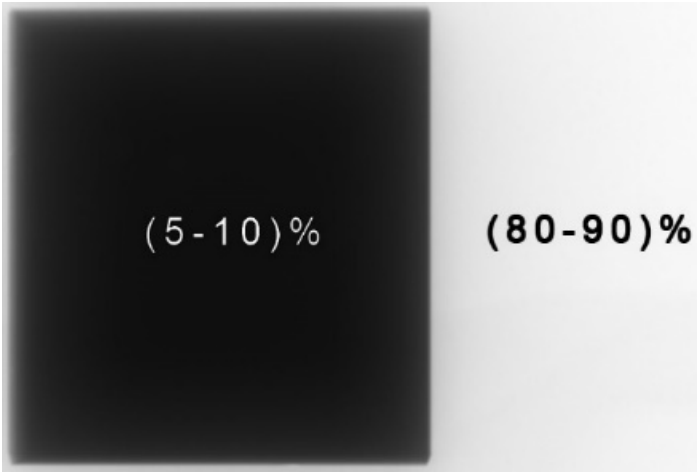

Fig. 2 Offset and gain corrected projection image through FeMnAl block (dark)

Table 1 XCT scanning parameters

X-ray voltage (peak)	450 kV
X-ray energy (peak)	450 keV
X-ray current	1550 µA
Detector sample rate	1 frame/s (fps)
X-ray focal spot size	400 µm
Source-to-image distance	875 mm
Source-to-object distance	575 mm
Magnification	1.52
Detector element pitch	200 µm
Effective pixel pitch	131 µm
Unsharpness	1.04 pixels
Frame average	4
No. of projections (views)	2200
Source filter (Cu)	15.9 mm (0.625 inch)

The detector field of view around the relatively dark block is unsaturated and has an intensity level of about 85% of maximum, or saturation level. The intensity level through the thickness of the block is only about 6%, well below the general 50% transmission rule of thumb. It is extremely difficult to distinguish any individual features or significant density variations in the single projection image, which has been frame averaged. The XCT scan method used four times frame averaging and projection image "oversampling" to maximize the detection of density variations within the FeMnAl blocks. When an image with random noise is frame averaged an n number of times, the magnitude of the noise fluctuation is decreased by the factor of the square root of n. In other words, the percent of original random noise remaining after n frames is averaged is $100 * (\frac{1}{\sqrt{n}})$.[6] It is evident from the functionality of this equation that as the number of frames increases, the improvement in noise reduction becomes less and less effective. Thus, although frame averaging does not add a large amount of processing time when applied to a

few images, such as a few digital radiographs, there is a tradeoff between improvement of images and processing time spent if a relatively large number of images will be averaged, such as is the case in extensive and/or oversampled XCT scans.

A commonly used number of frames averaged is four, which reduces noise fluctuation by 50%, because it significantly reduces the noise level in a reasonable amount of processing time for large data sets. In Nyquist–Shannon sampling theory,[7] given a polychromatic (i.e., multiple frequency) temporal (or spatial) continuous function, f(x), with known maximum spatial frequency X_{max}, it is completely determined by giving its sampled ordinates at a series of points spaced less than or equal to a distance of $1/(2X_{max})$ apart. The threshold $2X_{max}$ is called the Nyquist rate and is an attribute of the continuous spatial input f(x) being sampled. The sample rate, R, must exceed the Nyquist rate for the samples to suffice to represent f(x). The threshold R/2 is called the Nyquist frequency and is an attribute of the sampling equipment. The number of projections used to reconstruct an XCT data set is one of the determining factors in image quality. Too large an interval between projections, or undersampling, results in the loss of accurate information about the physical geometry of the scanned object. Reconstructed images of undersampled FeMnAl blocks would likely exhibit some type of regular angular variation in gray levels and associated loss of internal and edge physical information. Oversampling the scan space provides finer physical geometric information for the reconstruction process and helps to mitigate the effects of very high X-ray attenuation and related noise in the resultant XCT data. The scans of the blocks purposely collected twice as many projections as normal, which is based on 1.5 times the pixel width of the specimen field of view, to oversample the scan space during the 360° rotation. Application of effective frame averaging and oversampling the scan space are illustrative of the principle of beginning analysis with the best quality XCT data set reasonably obtainable given the material of interest and overall scan considerations.

4. XCT Results

4.1 Block Set A Results

Block set A includes blocks A1 to A4 (A1 was not available for XCT scanning). The physical 3-D locations of the images in the blocks and the order in which they are presented are designed to provide an overall understanding of the relative quality of the blocks. The directional perspectives of the front, side, and top view images are defined by the XCT scan geometry of the interior of each block. The front views are in the 50.8-mm (2-inch)-thick direction, with the geometric front

and back surfaces defined by the X-ray source and detector facing sides, respectively, at the start of the XCT scans. The side views are looking from the right- to the left-hand side of the blocks, with right and left defined by the X-ray source front surface perspective. The top views are looking down at the horizontal top surfaces (76.2 × 50.8 mm/ 3 × 2 inches) of the blocks.

4.1.1 Block A2

As can be seen in Figs. 3–6, block A2 has very little detectable porosity or void content. The top-left image in Fig. 6 shows some porosity near the back of the block and a medium-sized void in the front-right area of the block. However, the front, side, and top view images without any discontinuity indications are much more typical of block A2.

Fig. 3 Front views (76.2 × 76.2 mm/ 3 × 3 inches) just inside (i.e., 1 or 2 mm) the front surface, about one-quarter of the way through, and about halfway through the block on the left, middle, and right, respectively

Fig. 4 Front view image of a small void indication (circled) in the interior of the block

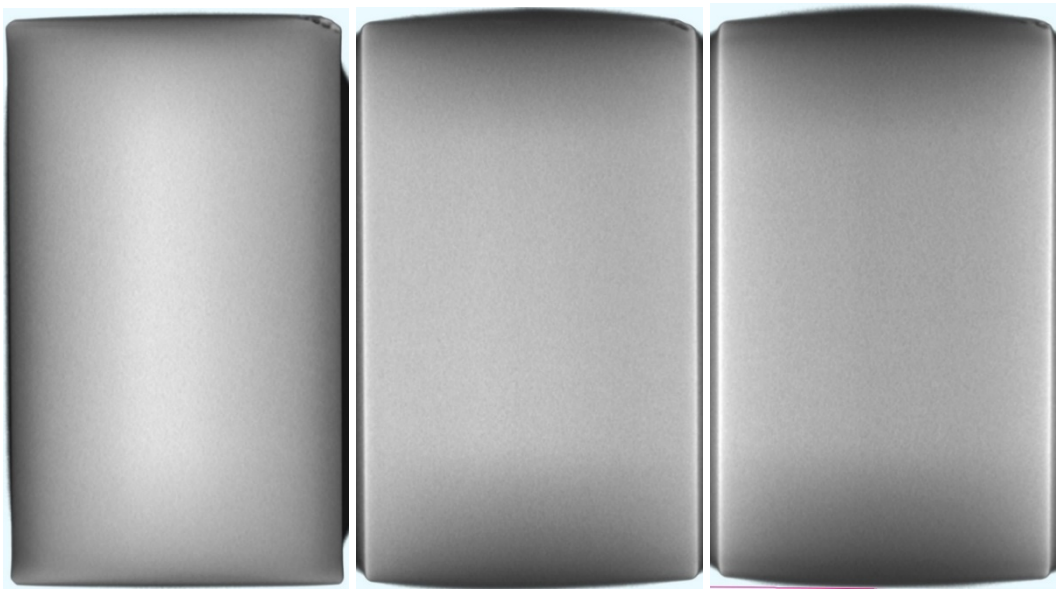

Fig. 5 Side views (50.8 × 76.2 mm/ 2 × 3 inches) just inside (i.e., 1 or 2 mm) the right-side surface, about one-quarter of the way through, and about halfway through the block on the left, middle, and right, respectively

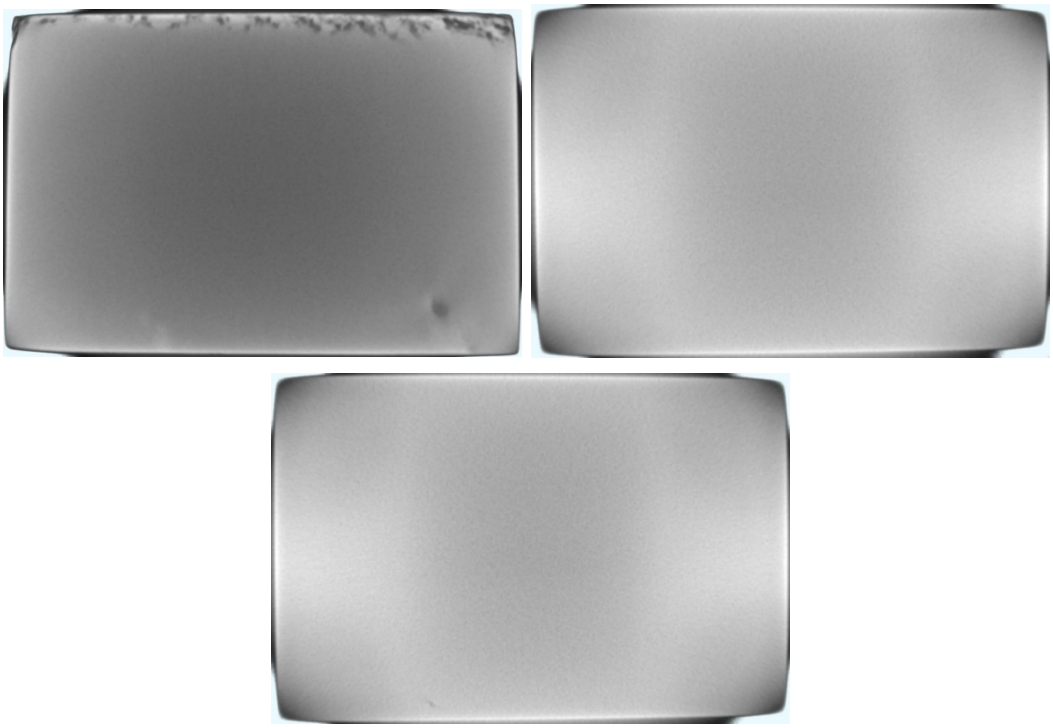

Fig. 6 Top views (76.2 × 50.8 mm/ 3 × 2 inches) just inside (i.e., 1 or 2 mm) the top surface, about one-quarter of the way through, and about halfway through the block on the top left, top right, and bottom, respectively

4.1.2 Block A3

As can be seen in Figs. 7–9, no discontinuities were detected in block A3, which is the highest-quality block in any set.

Fig. 7 Front views just inside the front surface, about one-quarter of the way through, and about halfway through the block on the left, middle, and right, respectively

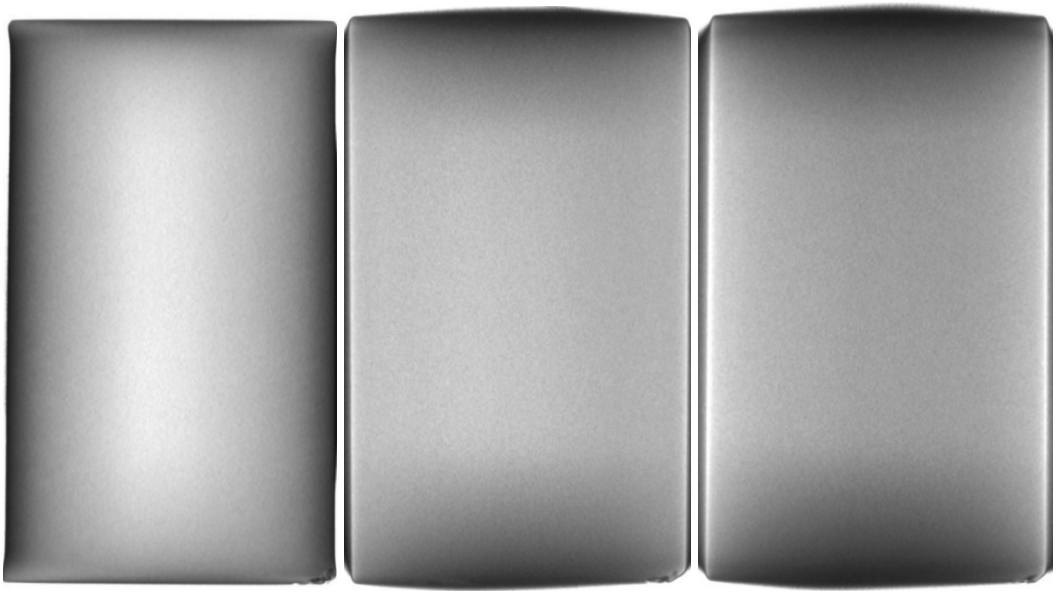

Fig. 8 Side views just inside the right-side surface, about one-quarter of the way through, and about halfway through the block on the left, middle, and right, respectively

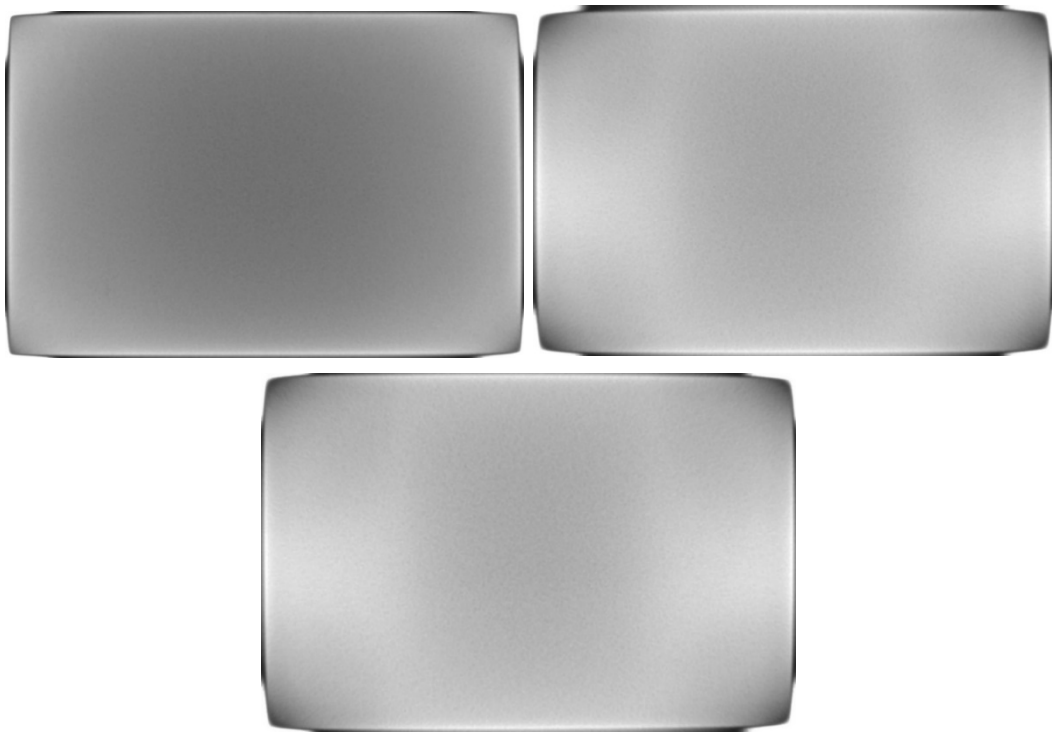

Fig. 9 Top views just inside the top surface, about one-quarter of the way through, and about halfway through the block on the top left, top right, and bottom, respectively

4.1.3 Block A4

As can be seen in Figs. 10–15, block A4 has some void content, but it is not severe, with only one larger and smaller void. The larger void is atypical of the A blocks in general.

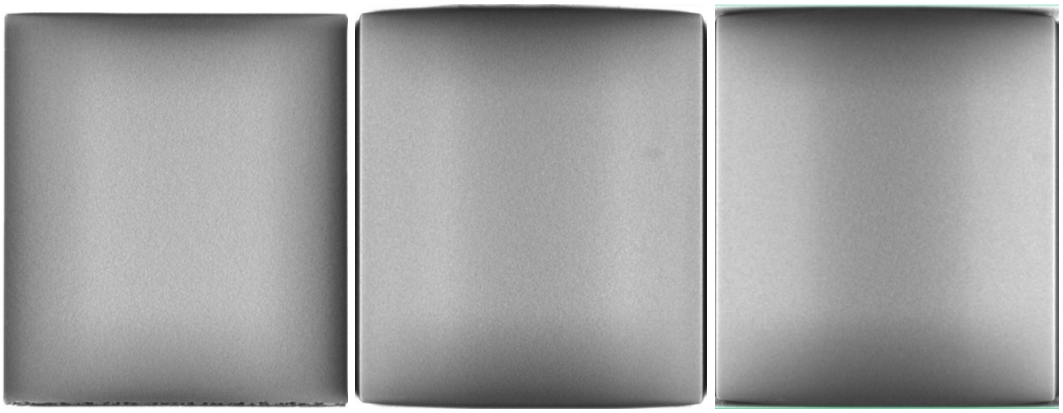

Fig. 10 Front views just inside the front surface, about one-quarter of the way through, and about halfway through the block on the left, middle, and right, respectively

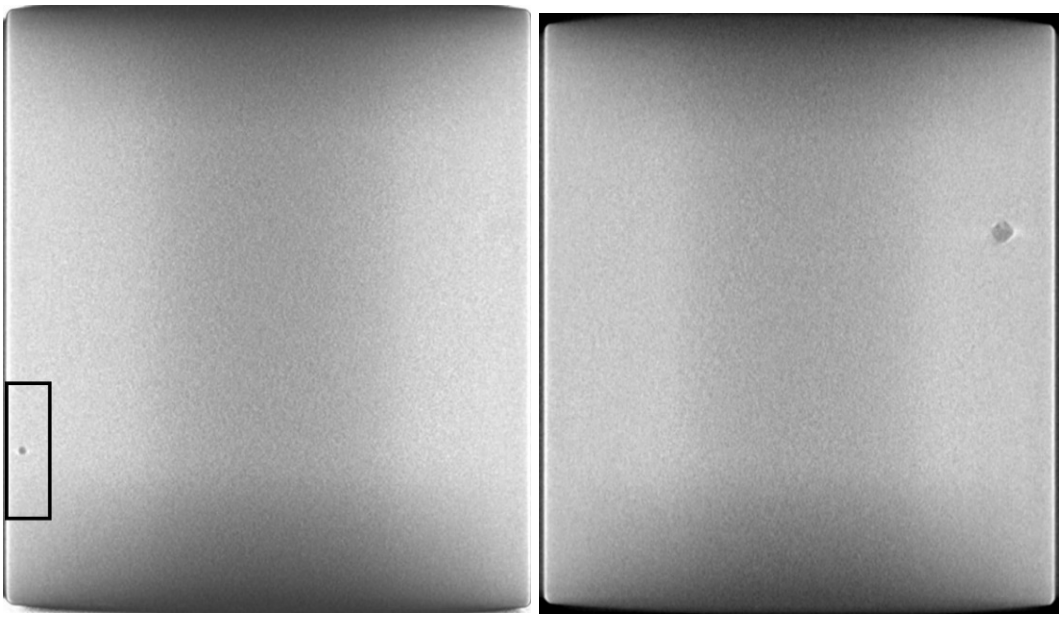

Fig. 11 Front view images of a small void (boxed) and a larger void about 3.0 × 3.2 mm (right side area) in the block on the left and right, respectively

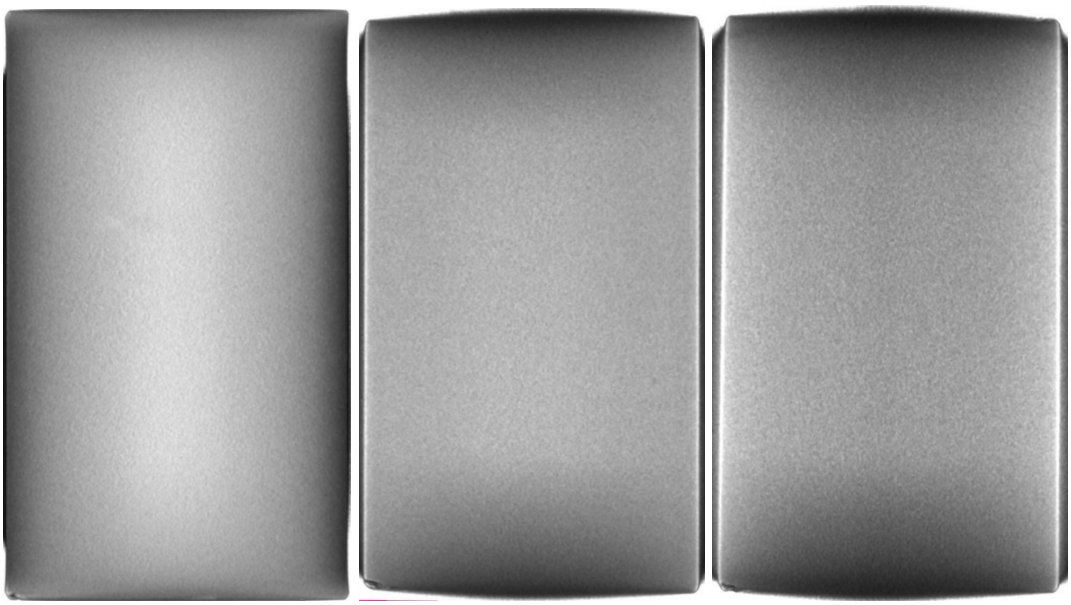

Fig. 12 Side views just inside the right-side surface, about one-quarter of the way through, and about halfway through the block on the left, middle, and right, respectively

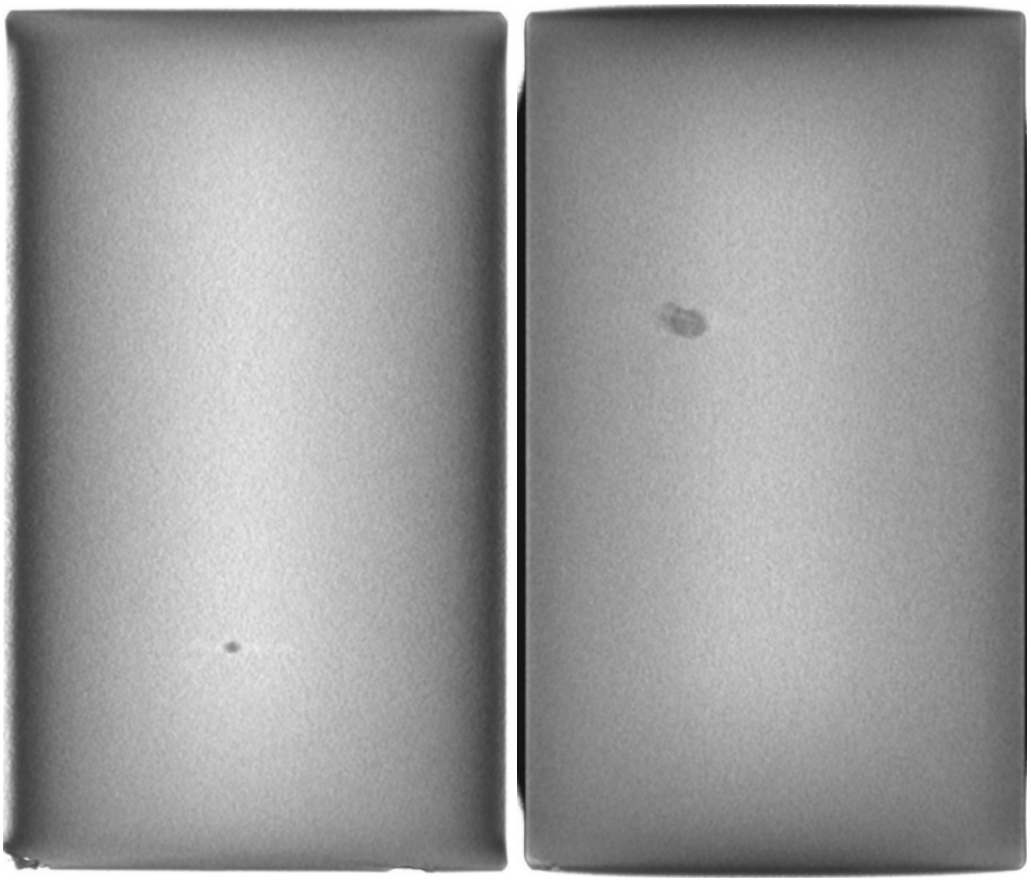

Fig. 13 Side view images of the smaller and larger void in the block on the left and right, respectively

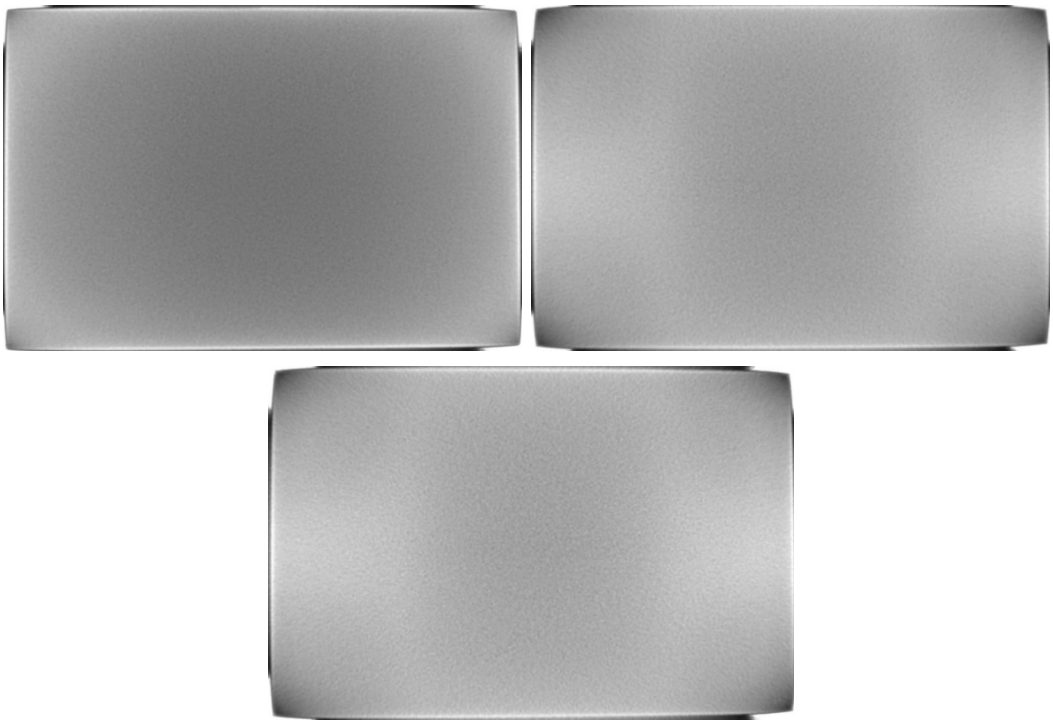

Fig. 14 Top views just inside the top surface, about one-quarter of the way through, and about halfway through the block on the top left, top right, and bottom, respectively

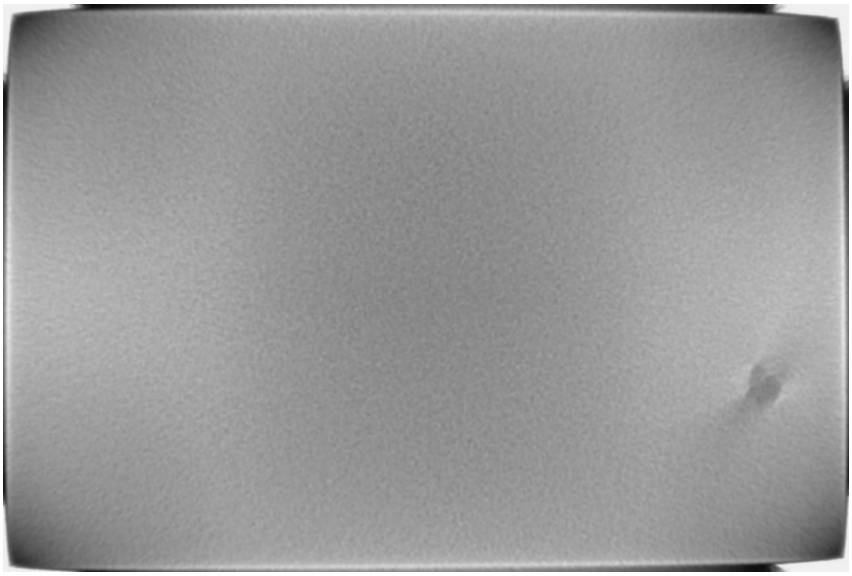

Fig. 15 Top view image of the larger void in the right side area of the block

4.2 Block Set B Results

Block set B includes the four blocks B1 to B4. The physical 3-D locations of the images in the blocks and the order in which they are presented are designed to provide an overall understanding of the relative quality of the blocks. The

directional perspectives of the front, side, and top view images are defined by the XCT scan geometry of the interior of each block.

4.2.1 Block B1

As can be seen in Figs. 16–20, block B1 has very little detectable porosity or void content, with only one detectable small void. However, block B1 is missing an extensive amount of material along one edge, as shown by the images on the left in Figs. 17 and 18. Each image shows an expanse of missing material on the right about one-half the height of the block, or 38.1 mm (1.5 inches) long, with varying width along the length on the order of several millimeters. The top view images in Fig. 20 also show indications of the missing material in their top-right corners. The front, side, and top view images without any porosity or void indications are typical of block B1.

Fig. 16 Front views (76.2 × 76.2 mm/ 3 × 3 inches) just inside the front surface, about one-quarter of the way through, and about halfway through the block on the left, middle, and right, respectively

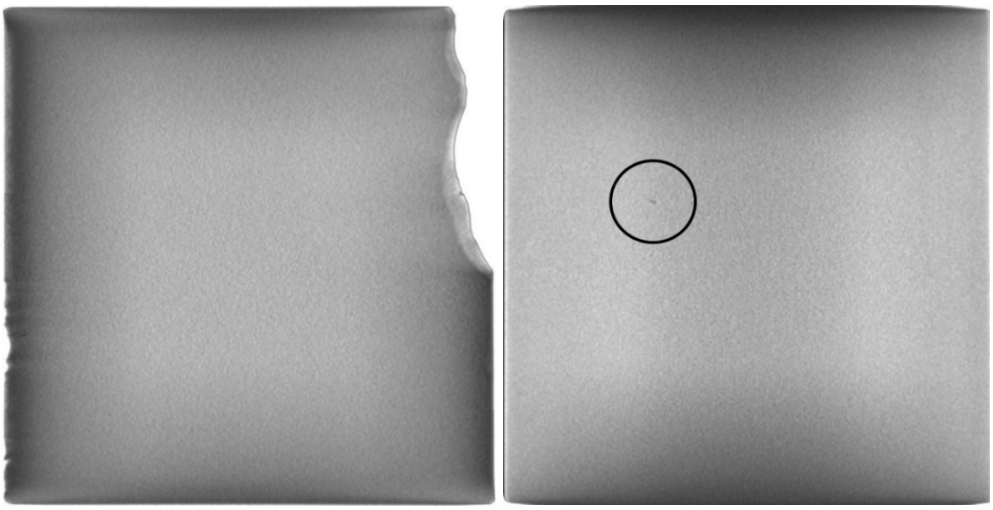

Fig. 17 Front view images near the back surface of the block and of a very small void indication on the left and right, respectively (void in right image is circled)

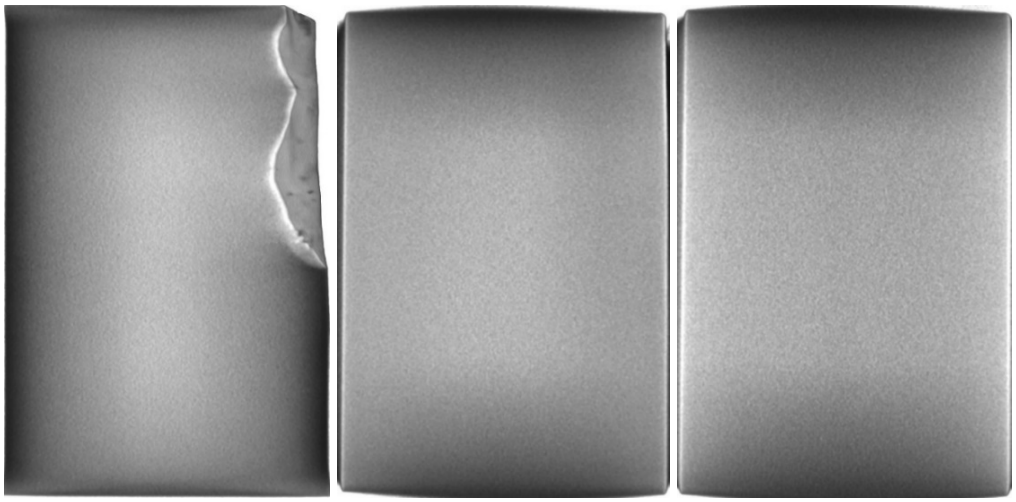

Fig. 18 Side views (50.8 × 76.2 mm/ 2 × 3 inches) just inside the right-side surface, about one-quarter of the way through, and about halfway through the block on the left, middle, and right, respectively

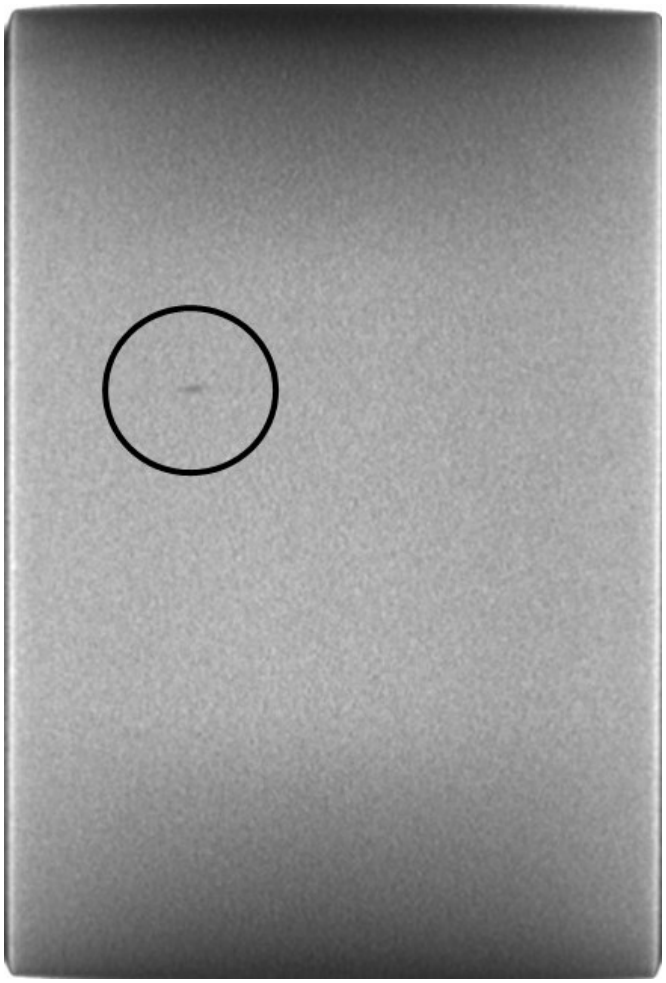

Fig. 19 Side view image of the very small void (circled) in the block

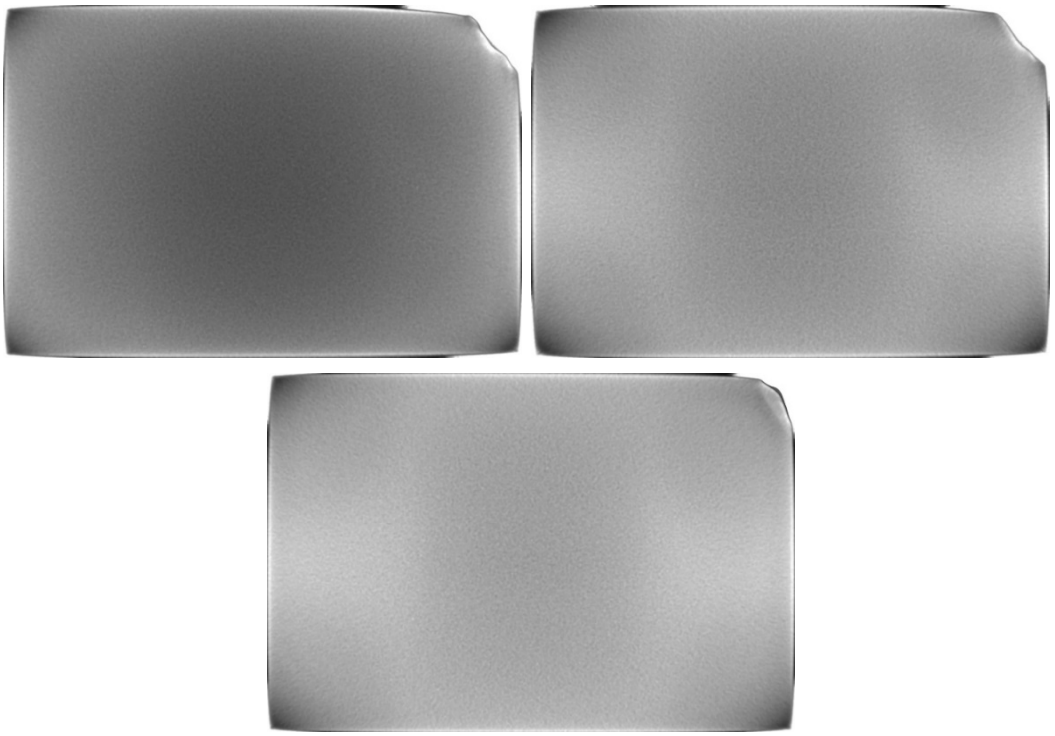

Fig. 20 Top views (76.2 × 50.8 mm/ 3 × 2 inches) just inside the top surface, about one-quarter of the way through, and about halfway through the block on the top left, top right, and bottom, respectively

4.2.2 Block B2

As can be seen in Figs. 21–25, block B2 has some small void and crack content, with the crack starting on the outside of the block. It is unknown if the crack or the full extent of it existed before the sectioning process, although this was not emphasized as an issue during sectioning. The crack is surrounded by black outlined boxes in the top two images of Fig. 25 due to both its shortness and faintness. Block B2 is also missing material in one corner as shown in Figs. 21 (left image, top right), 22 (left image, top left), and 24 (top left image, bottom right).

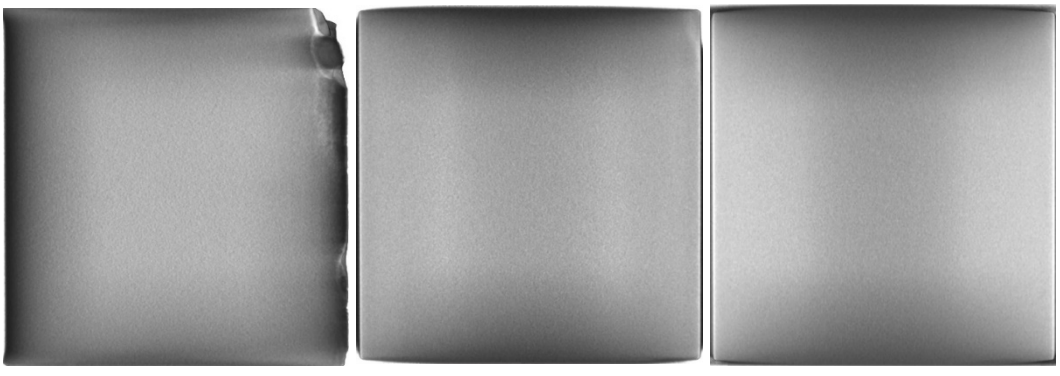

Fig. 21 Front views just inside the front surface, about one-quarter of the way through, and about halfway through the block on the left, middle, and right, respectively

Fig. 22 Side views just inside the right-side surface, about one-quarter of the way through, and about halfway through the block on the left, middle, and right, respectively

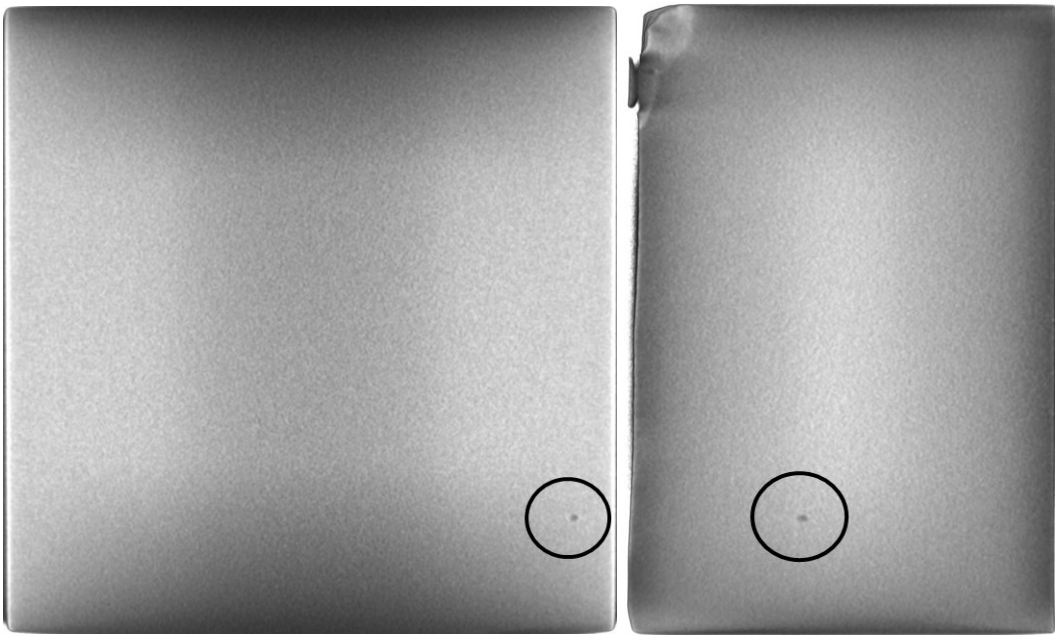

Fig. 23 Front and side view images of a small void indication (circled) in the block on the left and right, respectively

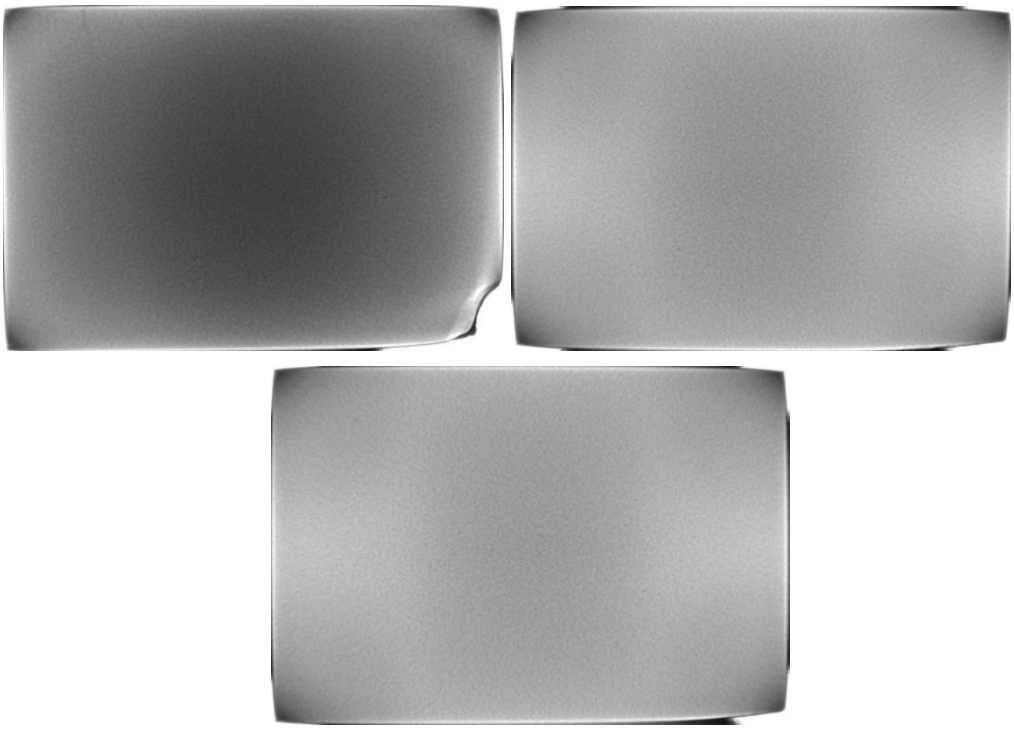

Fig. 24 Top views just inside the top surface, about one-quarter of the way through, and about halfway through the block on the top left, top right, and bottom, respectively

Fig. 25 Front, side, and top view images of a small crack in the block on the top left (boxed), top right (boxed), and bottom (not boxed), respectively. The crack in the top view (bottom image) is in the upper-left area of the image.

4.2.3 Block B3

As can be seen from Figs. 26–30, block B3 has no detectable porosity or voids and a small crack. Again, it is unknown if the crack or the full extent of it existed before the sectioning process. The crack is surrounded by black outlined boxes in the right image of Fig. 27 and the left image of Fig. 30 due to both its shortness and faintness. It is also boxed in the right image of Fig. 30. Block B3 is also missing material along one edge as shown in the images on the left in Figs. 27 and 28 on the right-hand side. The top-right image in Fig. 29 also shows missing material in the top-right corner.

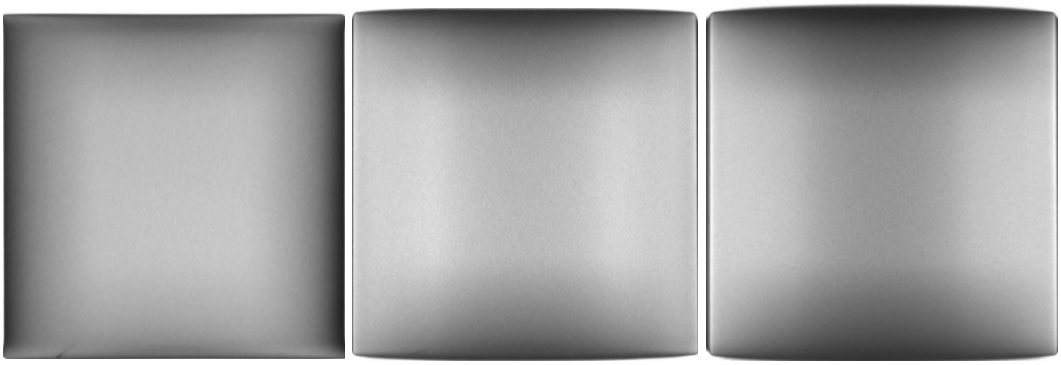

Fig. 26 Front views just inside the front surface, about one-quarter of the way through, and about halfway through the block on the left, middle, and right, respectively

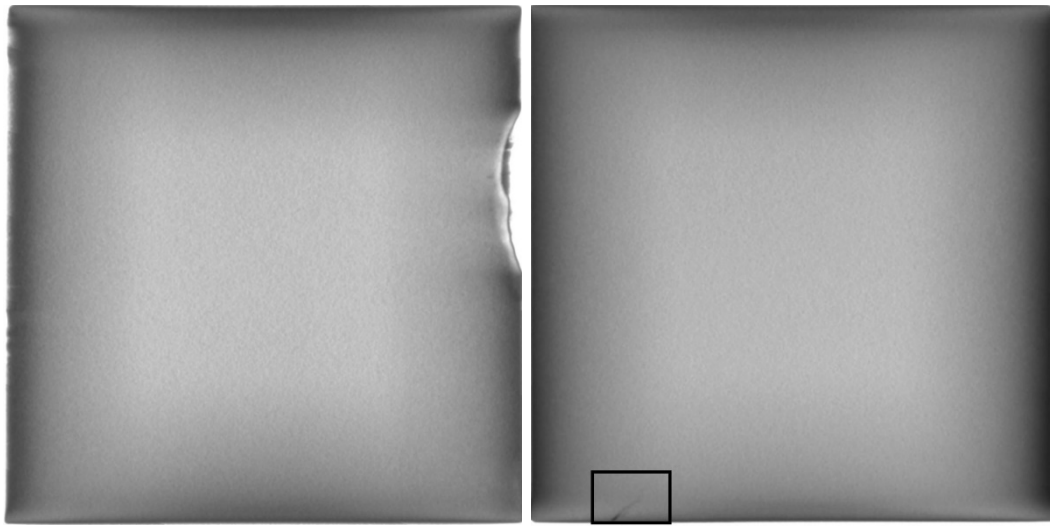

Fig. 27 Front view images near the back surface of the block and of a small crack in the block on the left and right, respectively. Crack in the lower-left corner area of right image is boxed.

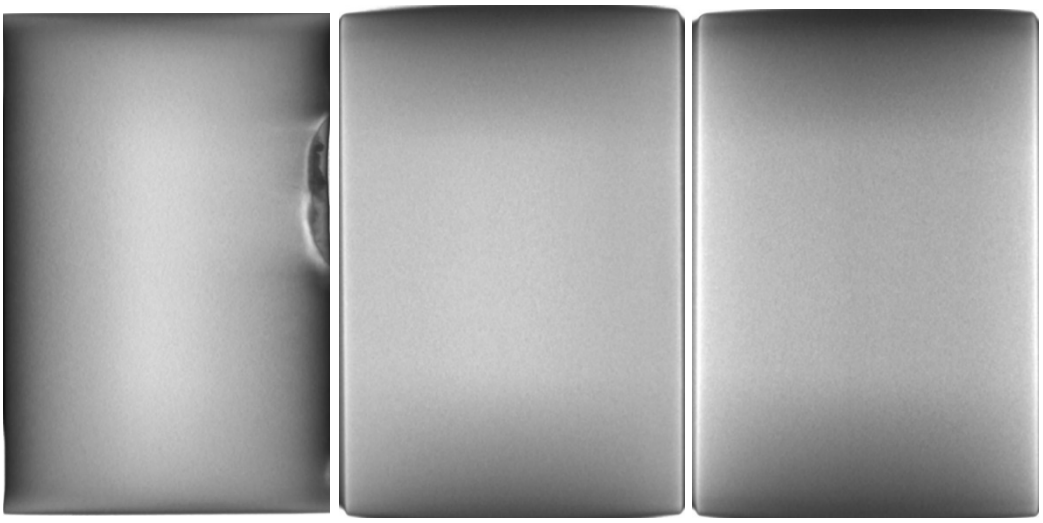

Fig. 28 Side views just inside the right-side surface, about one-quarter of the way through, and about halfway through the block on the left, middle, and right, respectively

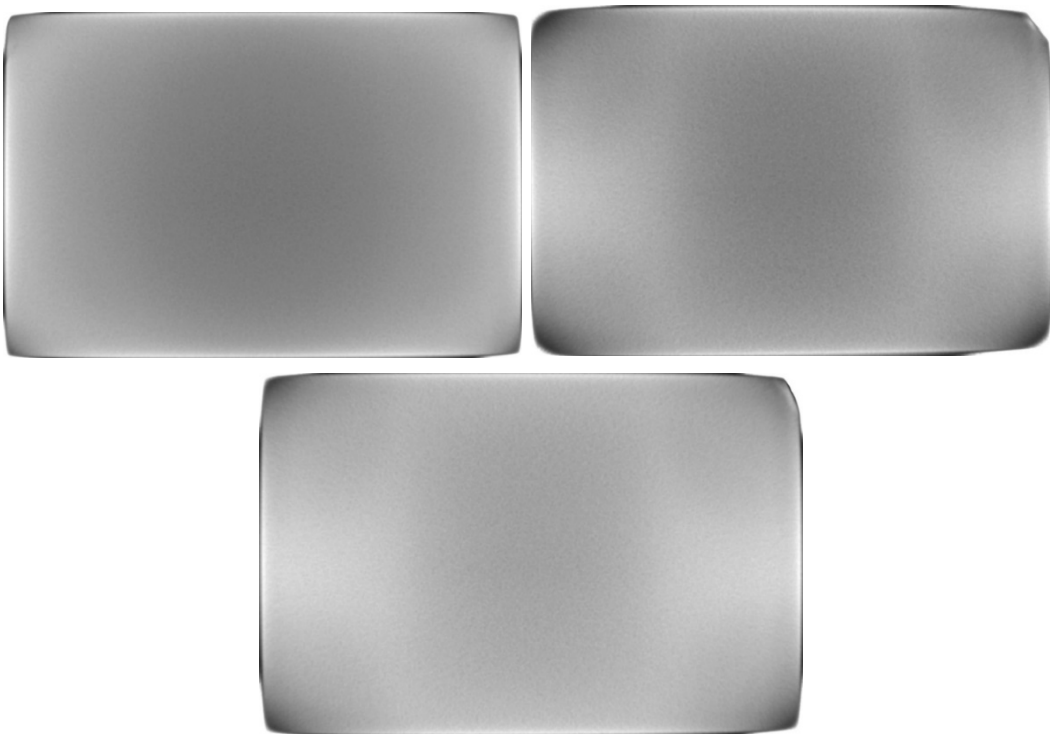

Fig. 29 Top views just inside the top surface, about one-quarter of the way through, and about halfway through the block on the top left, top right, and bottom, respectively

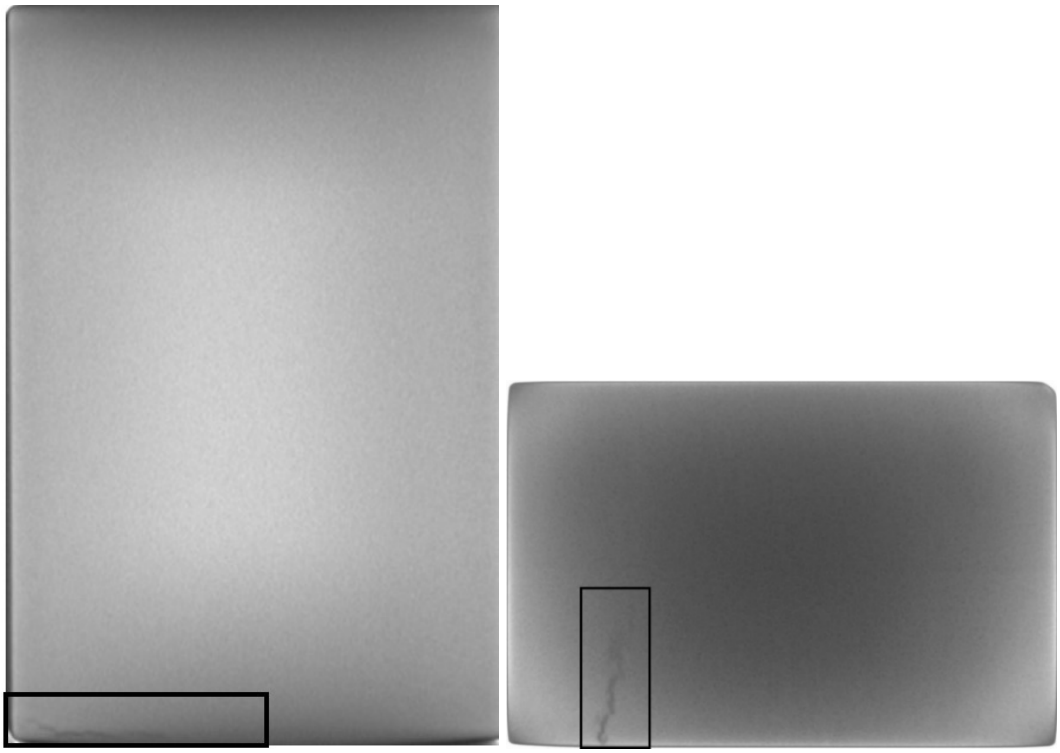

Fig. 30 Side and top view images of the small crack (boxed) in the block on the left and right, respectively

4.2.4 Block B4

As can be seen in Figs. 31–37, block B4 has some small void and crack content, with the crack starting on the outside of the block. It is unknown if the crack or the full extent of it existed before the sectioning process. The crack is surrounded by black outlined boxes in Fig. 37 due to both its shortness and faintness. Small void indications are shown and circled in Figs. 32, 34, and 36. Block B4 is the only B block without missing material along an edge or at a corner, and it does not have extensive porosity or void content. Blocks B1, B2, and B4 all have detectable small voids. Blocks B2, B3, and B4 all have a small crack, which may have been present in whole or in part before the sectioning process. Blocks B1, B2, and B3 are all missing expanses of material along an edge or at a corner. Block set B is considered to be of lower overall quality than block set A as determined by the number of detectable discontinuity features and their severity.

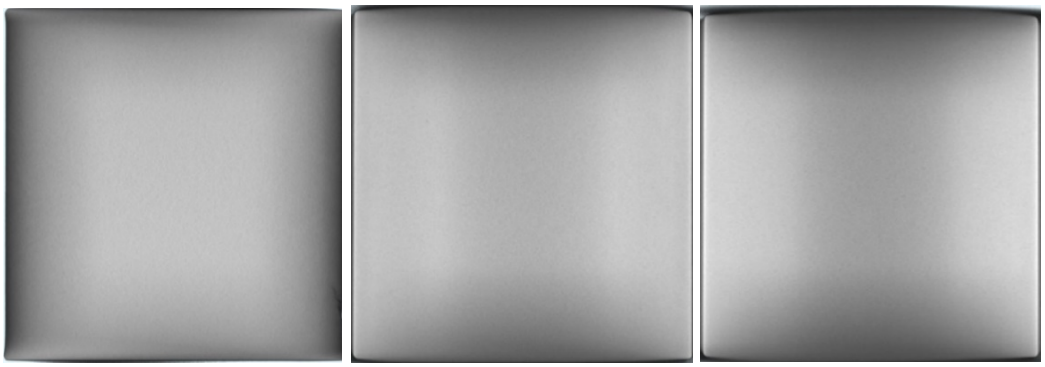

Fig. 31 Front views just inside the front surface, about one-quarter of the way through, and about halfway through the block on the left, middle, and right, respectively

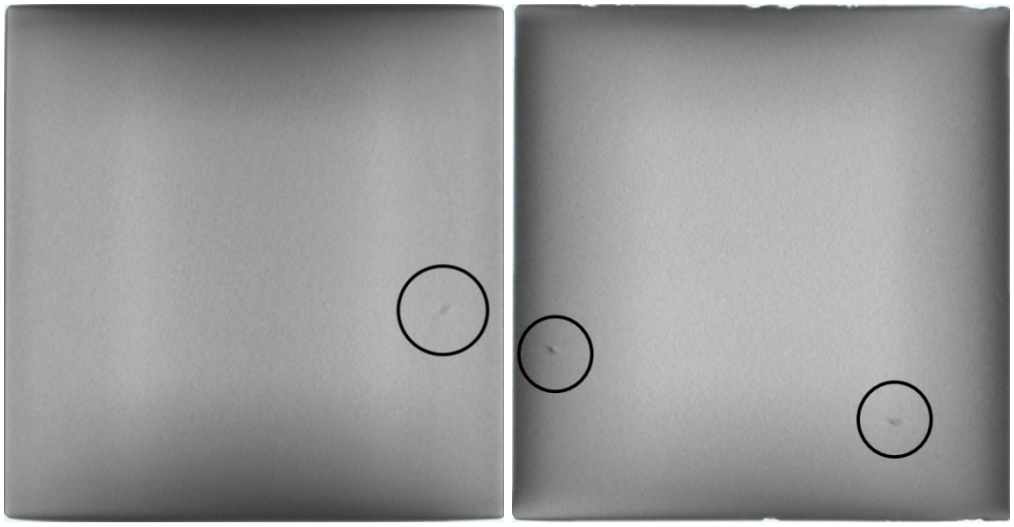

Fig. 32 Two front view images of different small void indications (circled) in the block

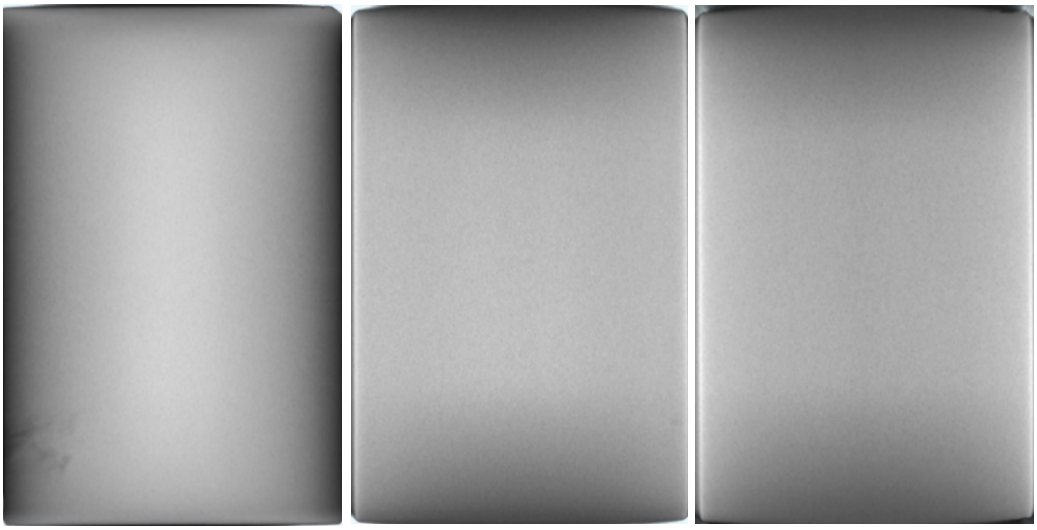

Fig. 33 Side views just inside the right-side surface, about one-quarter of the way through, and about halfway through the block on the left, middle, and right, respectively

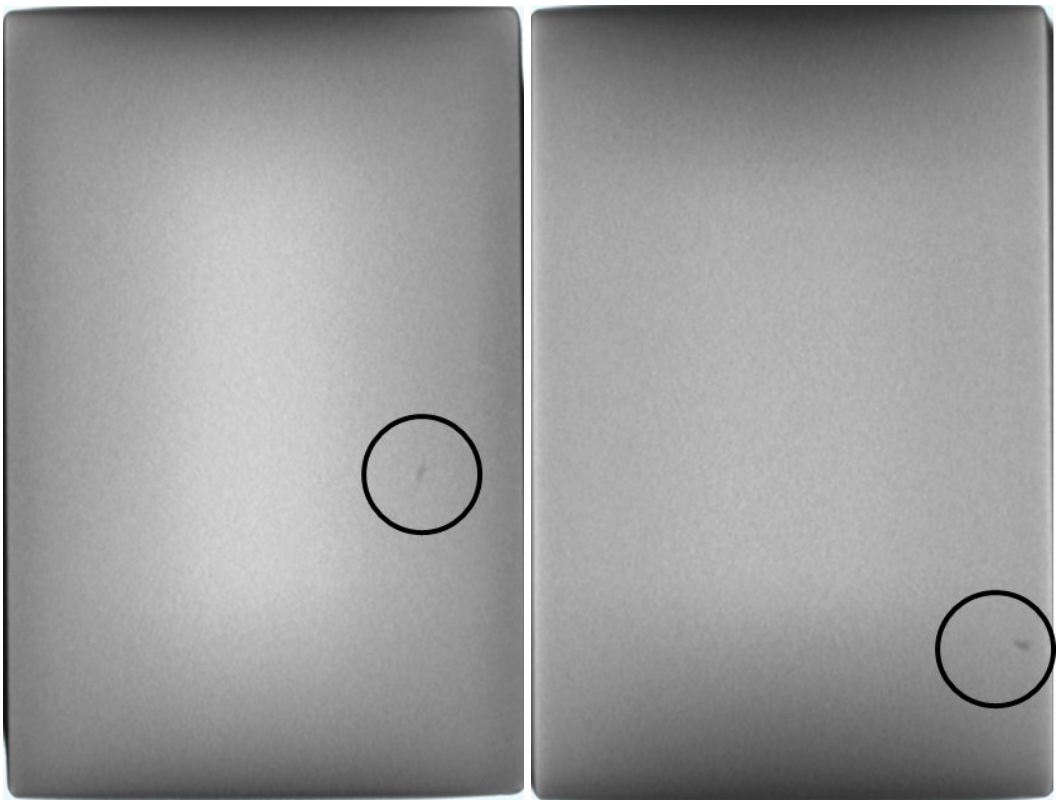

Fig. 34 Two side view images of different small void indications (circled) in the block

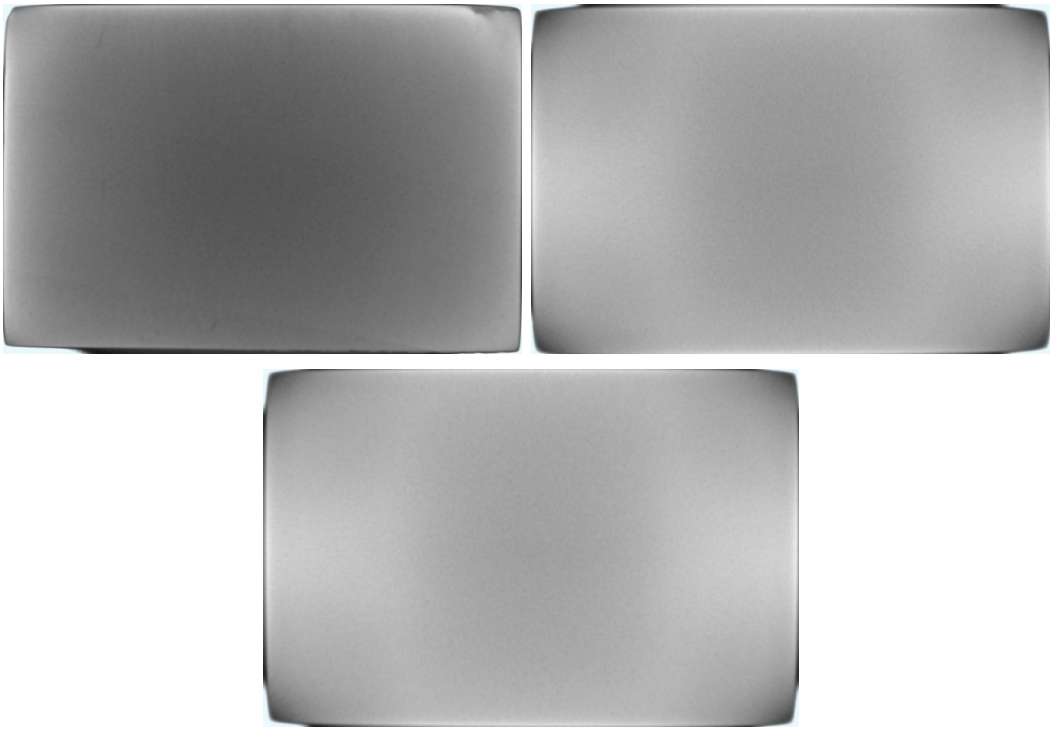

Fig. 35 Top views just inside the top surface, about one-quarter of the way through, and about halfway through the block on the top left, top right, and bottom, respectively

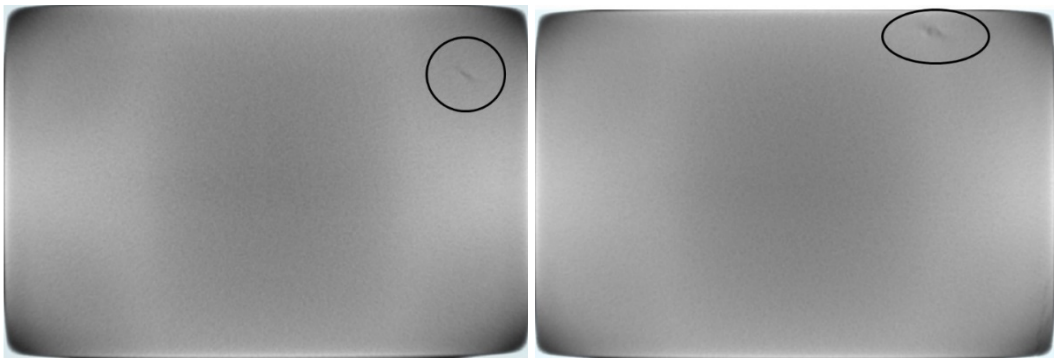

Fig. 36 Two top view images of different small void indications (circled) in the block

Fig. 37 Front and top view images of a small crack (boxed) in the block starting from the outside

4.3 Block Set C Results

Block set C includes the six blocks C1 to C6, of which C1 was already mechanically rolled before XCT scanning. The physical 3-D locations of the images in the blocks and the order in which they are presented are designed to provide an overall understanding of the relative quality of the blocks. The directional perspectives of the front, side, and top view images are defined by the XCT scan geometry of the interior of each block. This grouping also contains double-sectioned 3-D images of large void features. These types of images often have vertical, horizontal, or slanted lines in them, indicating physical locations of "cutting", or sectioning, planes, which are used to virtually remove any amount of material, leaving only that which is desired to be viewed, such as multiple planar dimensions of a void. In this case, the descriptions will start with blocks C2 to C6; block C1 will be discussed last because reviewing the detectable features in blocks C2 to C6 will provide a better understand of the features in C1. Block C1 was the only block mechanically rolled before scanning.

4.3.1 Block C2

Block C2 (Figs. 38–43) has relatively large and extensive porosity and void features readily apparent within it as the figures show, unlike the A and B block sets. The front, side, and top view images near the outer surfaces of the block all have discernible extended and asymmetric, or more crack-like or dendritic, type porosity features, again unlike the A and B block sets. The front, side, and top view images also have some of these crack-like or dendritic features one-quarter and three-quarters of the way through the thickness of the block in their respective directions. However, the same views located at about the center of the block, as well as the views of the large void, have more rounded or symmetric and less extended, dendritic features. The large void shown in Fig. 39 (top-right image, bottom side) has approximate dimensions of 5.4 mm (0.21 inch) × 5.8 mm (0.23 inch). The nature of the porosity and voids in block C2 clearly changed from extended and asymmetric, or more crack-like, features nearer to the outside of the block to significantly more rounded or symmetric pores or void features in the center region of the block, the edge or side void notwithstanding. Block C2 is also one of the C blocks with a sizable edge or corner void.

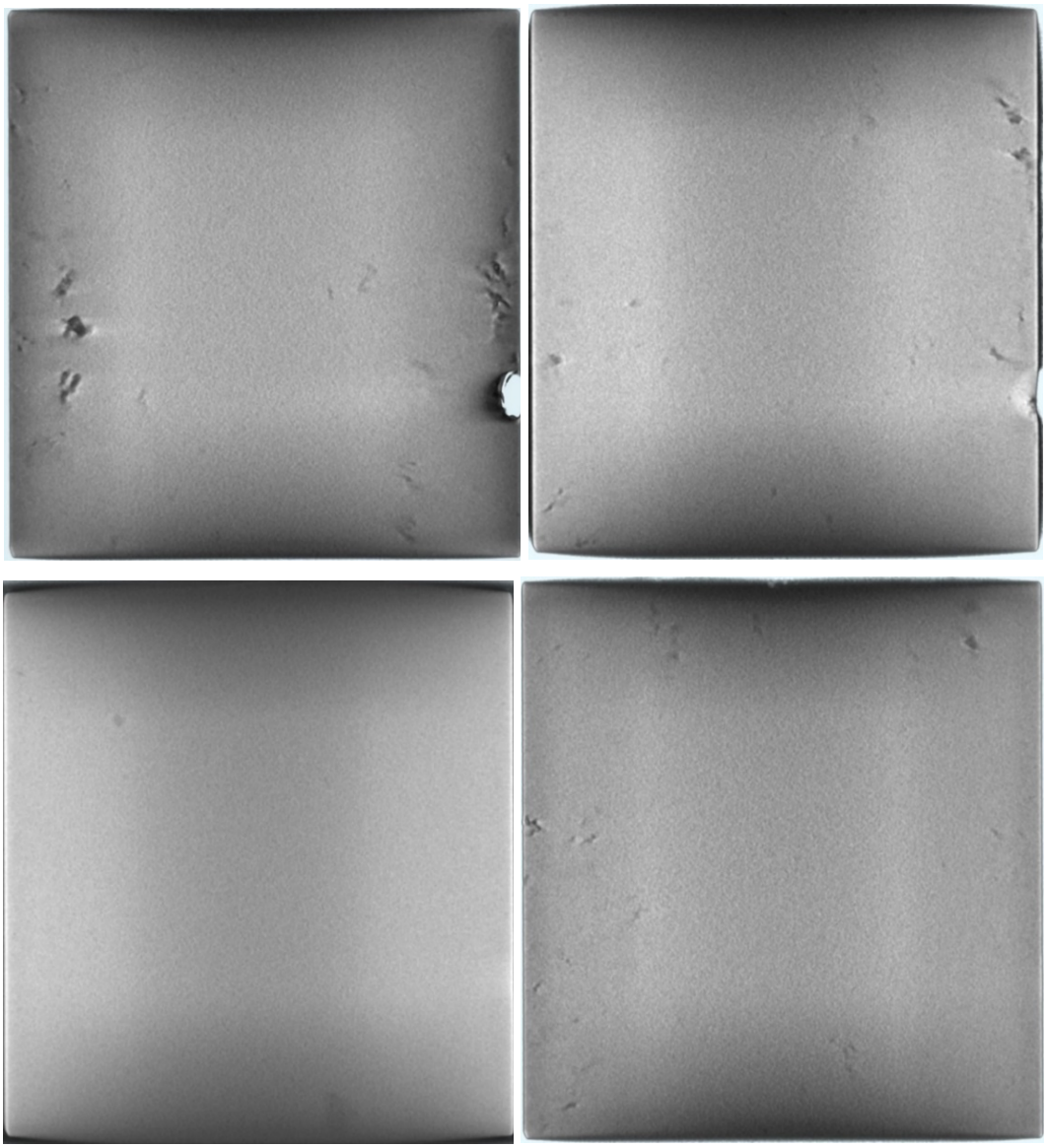

Fig. 38 Front views (76.2 × 76.2 mm/ 3 × 3 inches) just inside the front surface and about one-quarter of the way, halfway, and three-quarters of the way through the block on the top left, top right, bottom left, and bottom right, respectively

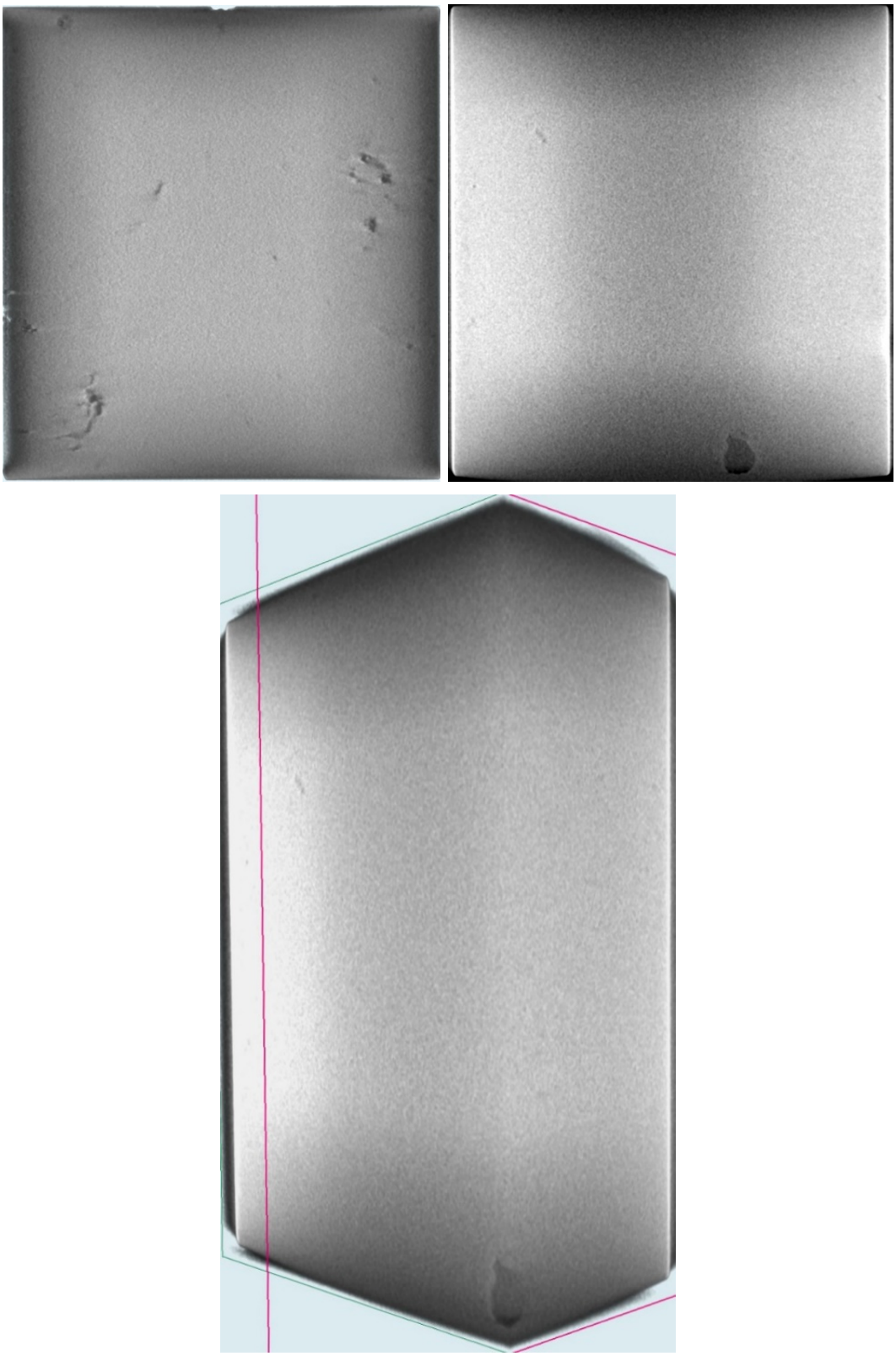

Fig. 39 Front view images near the back surface of the block and of a large void in the block on the top left and right, respectively; double-sectioned 3-D view of the large void in the lowest corner area of the block (bottom image)

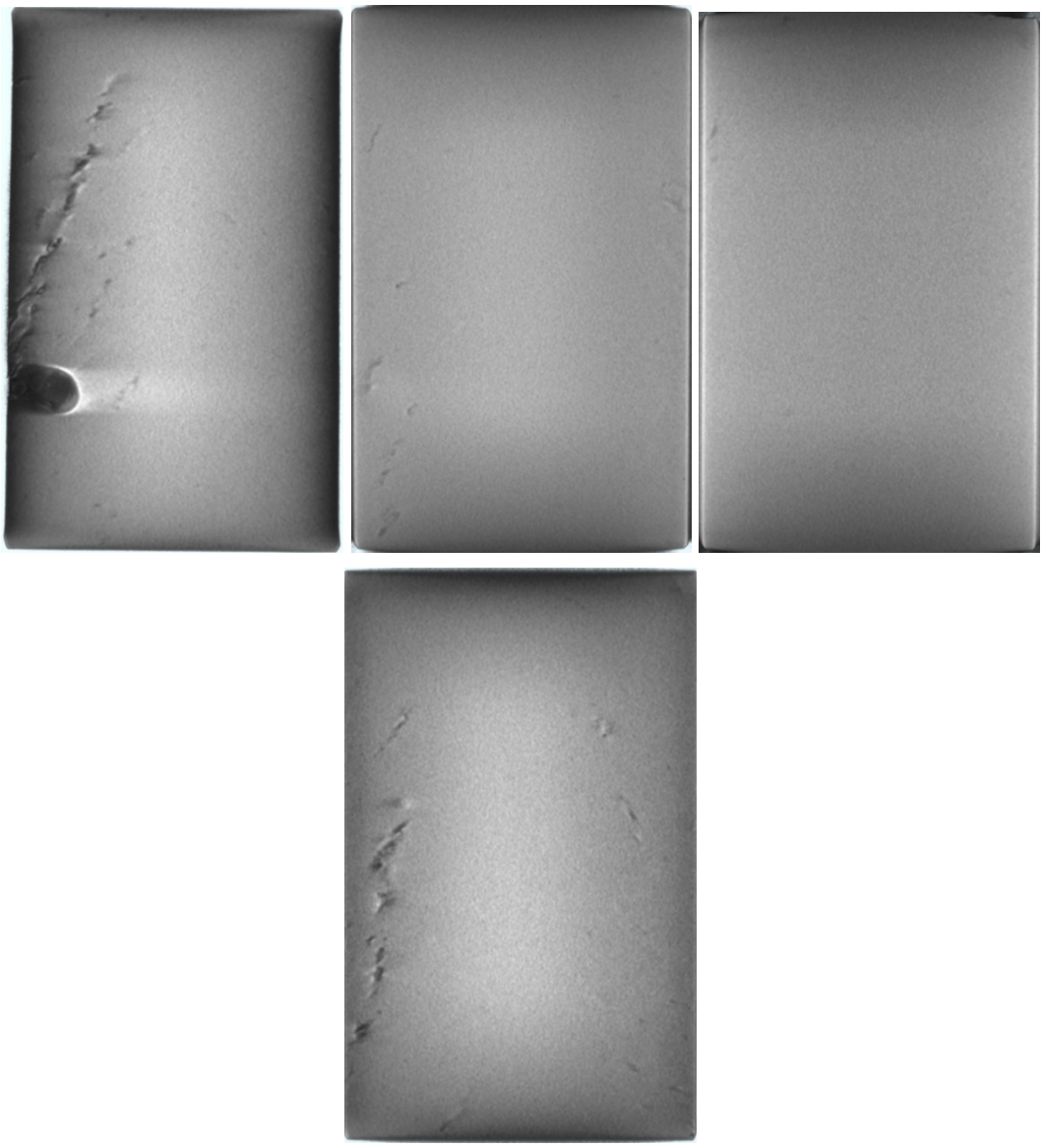

Fig. 40 Side views (50.8 × 76.2 mm/ 2 × 3 inches) just inside the right-side surface and about one-quarter of the way, halfway, and three-quarters of the way through the block on the top left, middle, and right, and bottom, respectively

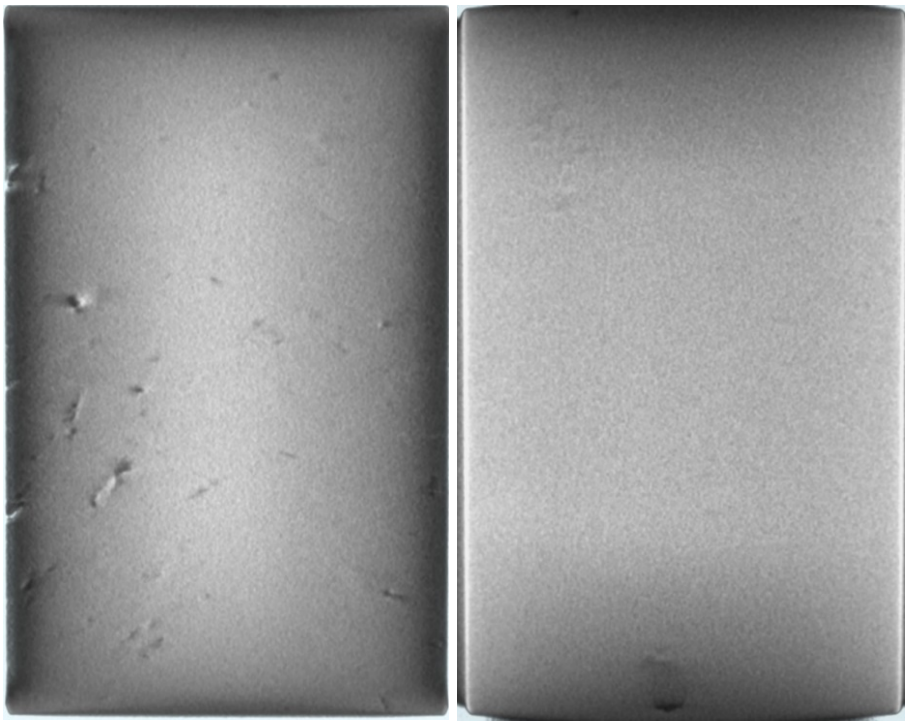

Fig. 41 Side view images near the left-side surface of the block and of the large void in the block (bottom area) on the left and right, respectively

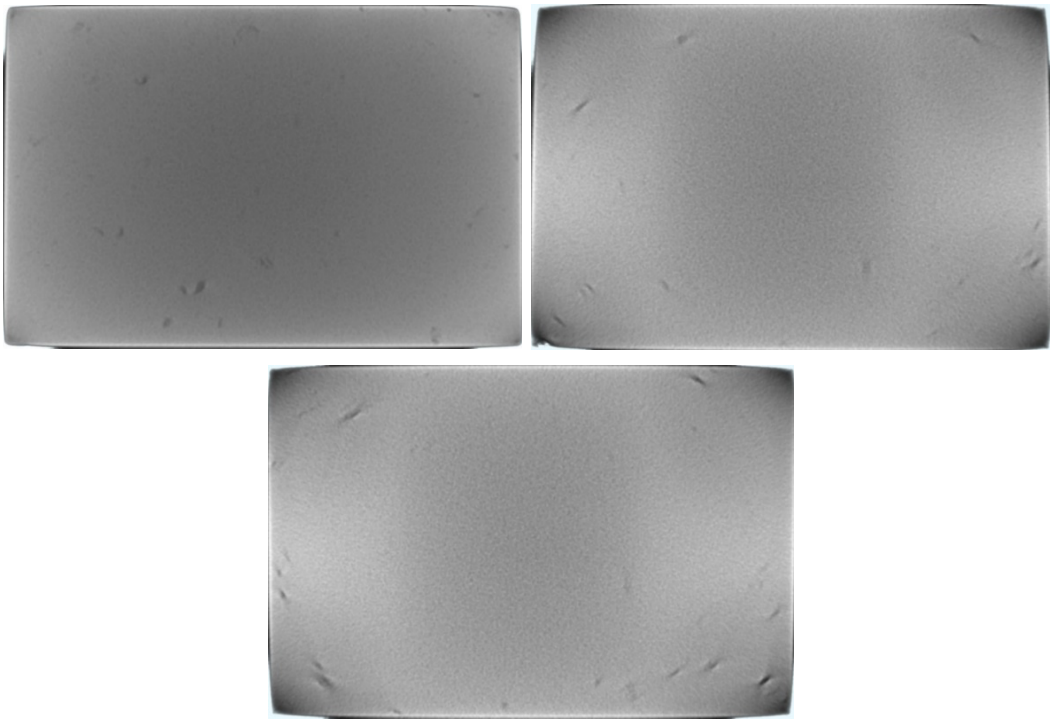

Fig. 42 Top views (76.2 × 50.8 mm/ 3 × 2 inches) just inside the top surface and about one-quarter of the way and halfway through the block on the top left, top right, and bottom, respectively

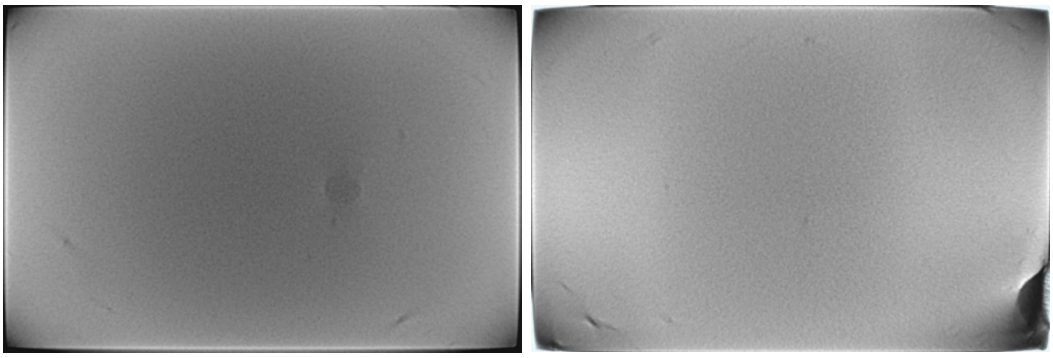

Fig. 43 Top view images of the large void and a different side void (bottom right area) in the block on the left and right, respectively

4.3.2 Block C3

As Figs. 44–48 show, the porosity and voids within block C3 are much like those within block C2, with C3 having a very large oval void (top-left image) about 6.8 mm (0.27 inch) × 8.1 mm (0.32 inch) and a different edge void (top-right image) both shown in Fig. 45. In fact, the presence of at least one relatively large void is typical in blocks C2–C6, and some of the blocks also have voids intersecting edges or corners created by the sectioning process as shown in Fig. 38 for block C2 (top-left image, right side), and Figs. 45 (top-right image, right side) and 46 (top-left image, right side) for block C3. Another feature in block C3 exhibited by the other C blocks in general is shown in Fig. 47, where the first two top view images (top left, top right) have approximately diagonal linear features very close to the corners of the block. Thus, there are relatively short linear porosity features in close proximity to corners in top views that are not too far from significantly more symmetric large voids.

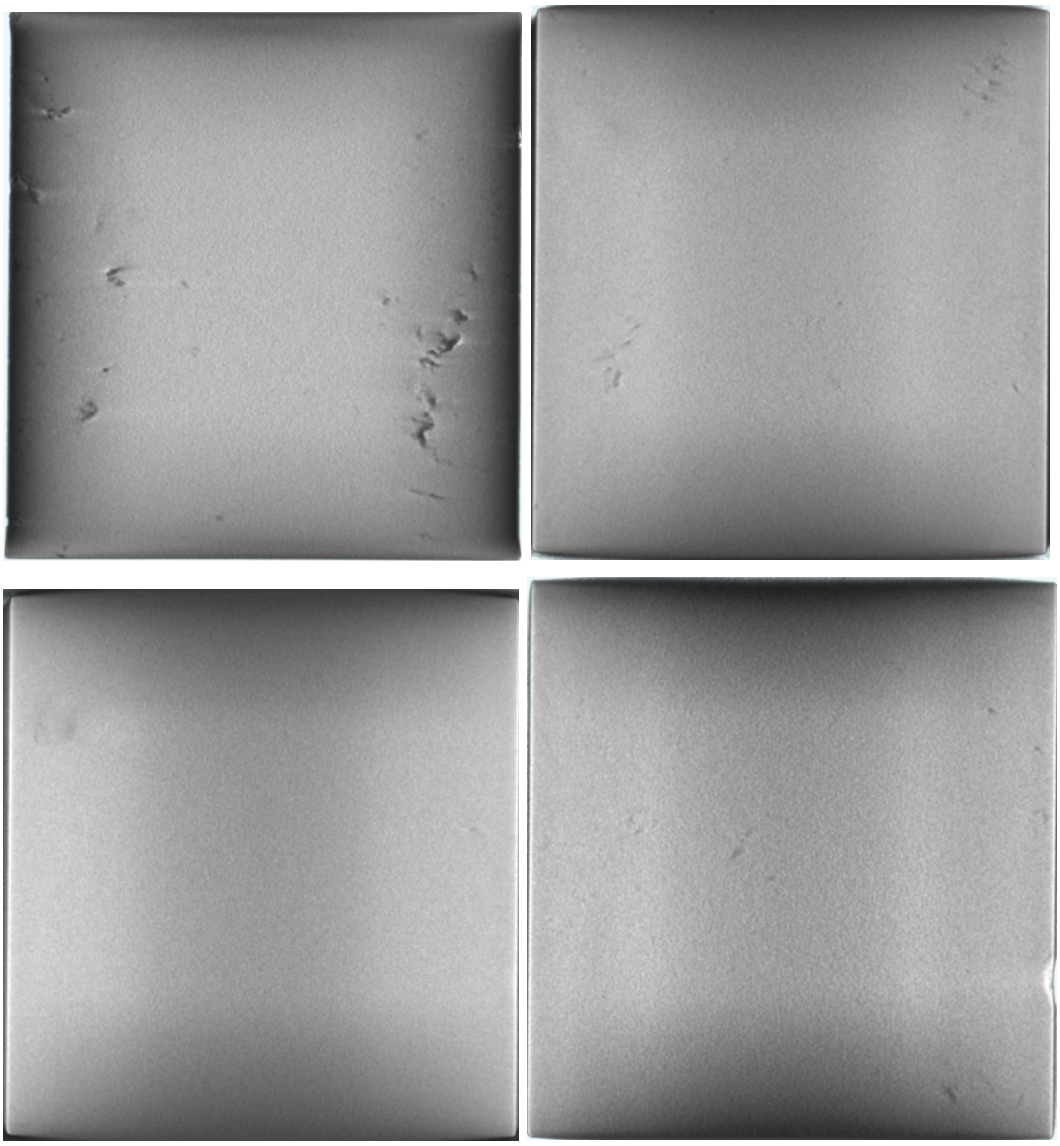

Fig. 44 Front views just inside the front surface and about one-quarter of the way, halfway, and three-quarters of the way through the block on the top left, top right, bottom left, and bottom right, respectively

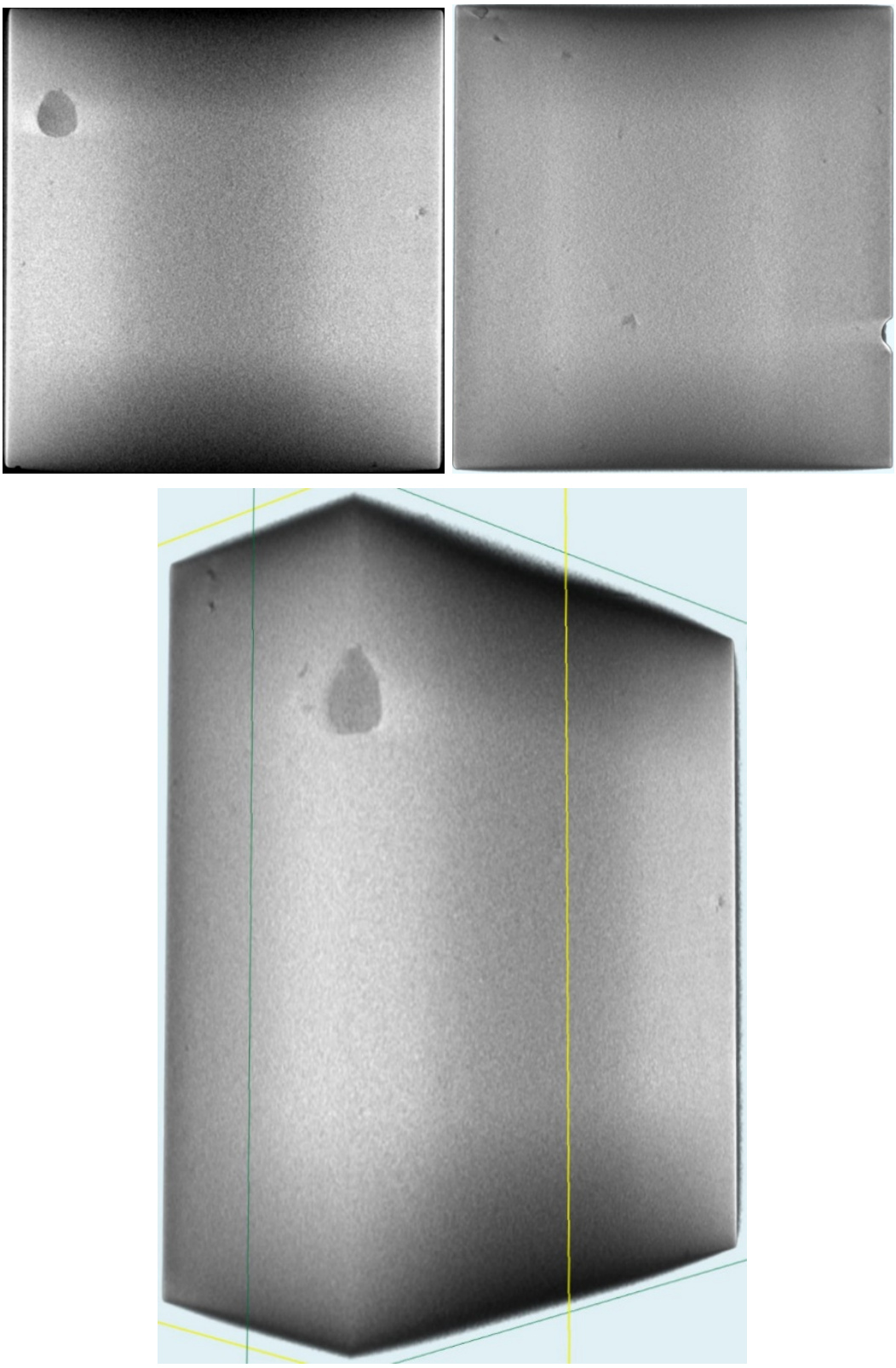

Fig. 45 Front view images of a very large void and a different corner void (right-hand side) in the block on the top left and right, respectively; double-sectioned 3-D view of the very large void (bottom image)

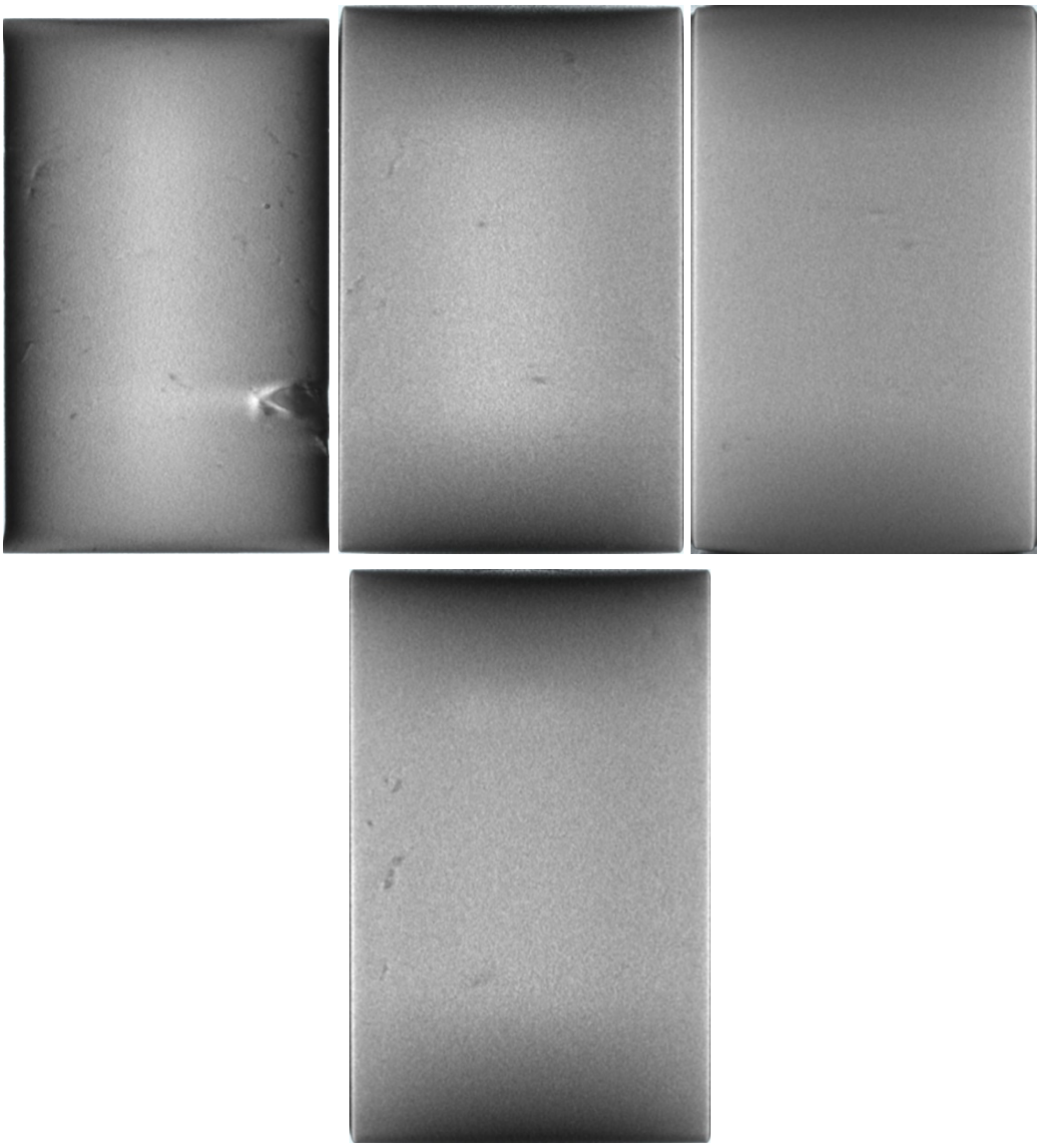

Fig. 46 Side views just inside the right-side surface and about one-quarter of the way, halfway, and three-quarters of the way through the block on the top left, middle, and right, and bottom, respectively

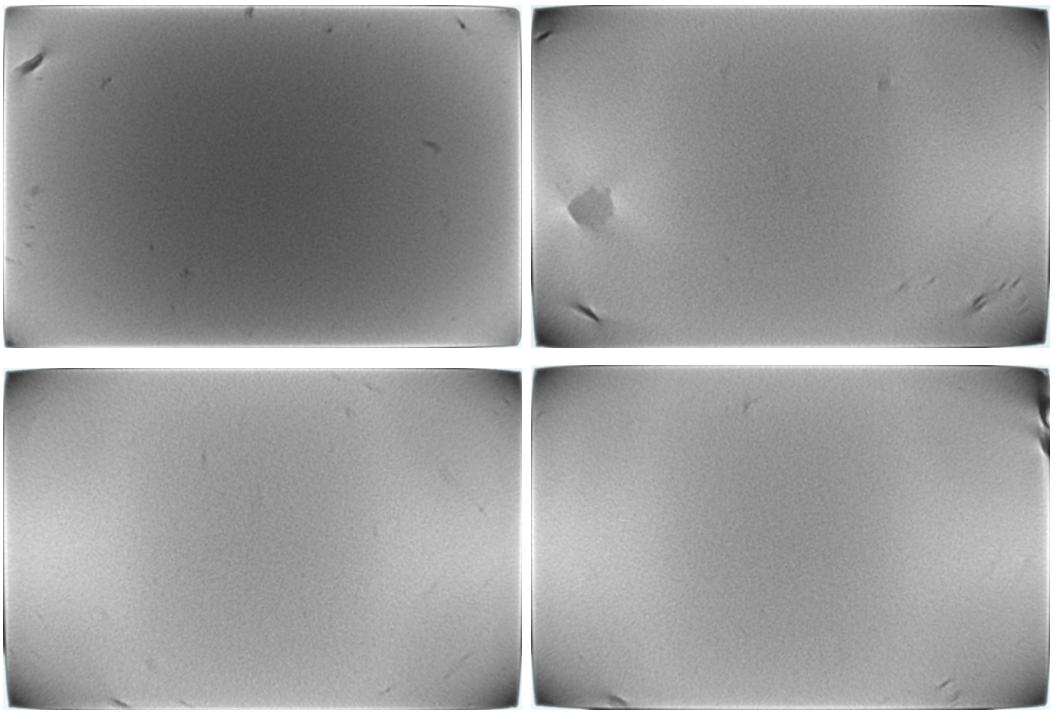

Fig. 47 Top views just inside the top surface and about one-quarter of the way, halfway, and three-quarters of the way through the block on the top left, top right, bottom left, and bottom right, respectively

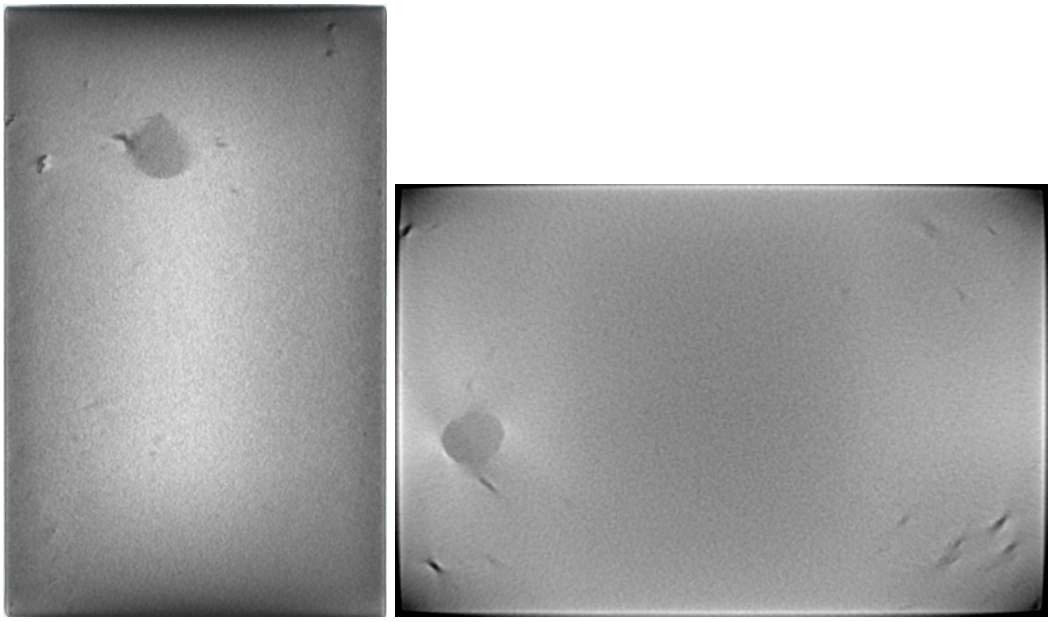

Fig. 48 Side and top view images of the very large void in the block on the left and right, respectively

4.3.3 Block C4

The extensive qualitative and quantitative evaluation of block C4 itself is thoroughly described in the CCDC Army Research Laboratory technical report ARL-TR-8975.[8] The report discusses porosity and void features as well as the advanced image-processing methodology used to determine quantitative porosity and void content in the interior of the block.

Again, the overall quality of block C4 and the severity of the porosity and voids within it are much like that within blocks C2 and C3. However, block C4 has two large voids relatively close together that are about the same size with diameters of roughly 6.5 mm (0.26 inch) as shown in Figs. 49–53. Figure 52 also shows the approximately diagonal linear features in close proximity to corners and the more symmetric and, in this case, centralized large voids in these top views.

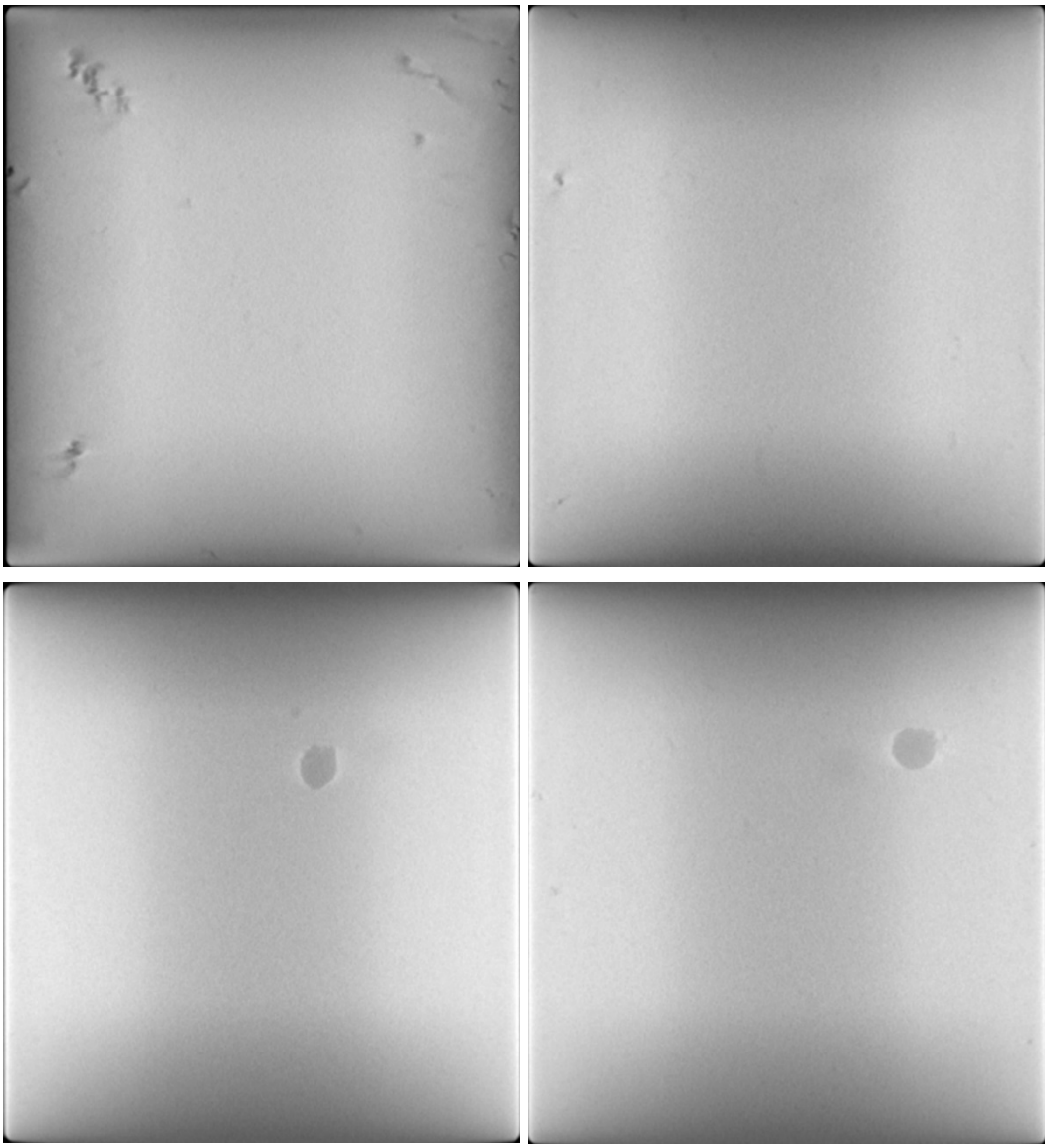

Fig. 49 Front views near the front surface, about halfway through, and of two different large voids in the block on the top left, top right, bottom left, and bottom right, respectively

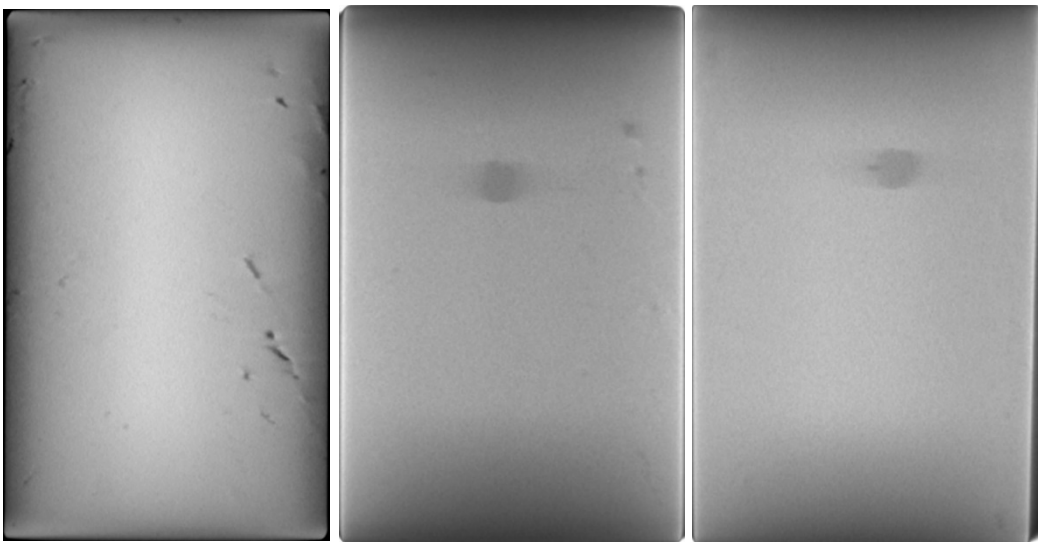

Fig. 50 Side views near the right-side surface and of the two large voids in the block on the left, middle, and right, respectively

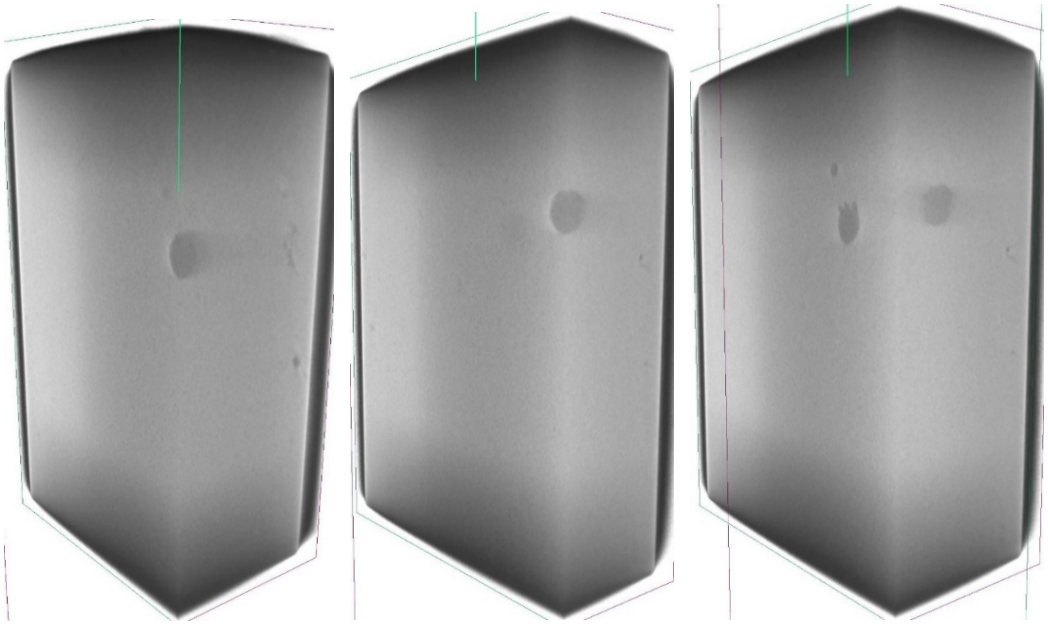

Fig. 51 Double-sectioned 3-D views of each large void individually and both voids together from the front-side perspective in the block on the left, middle, and right, respectively

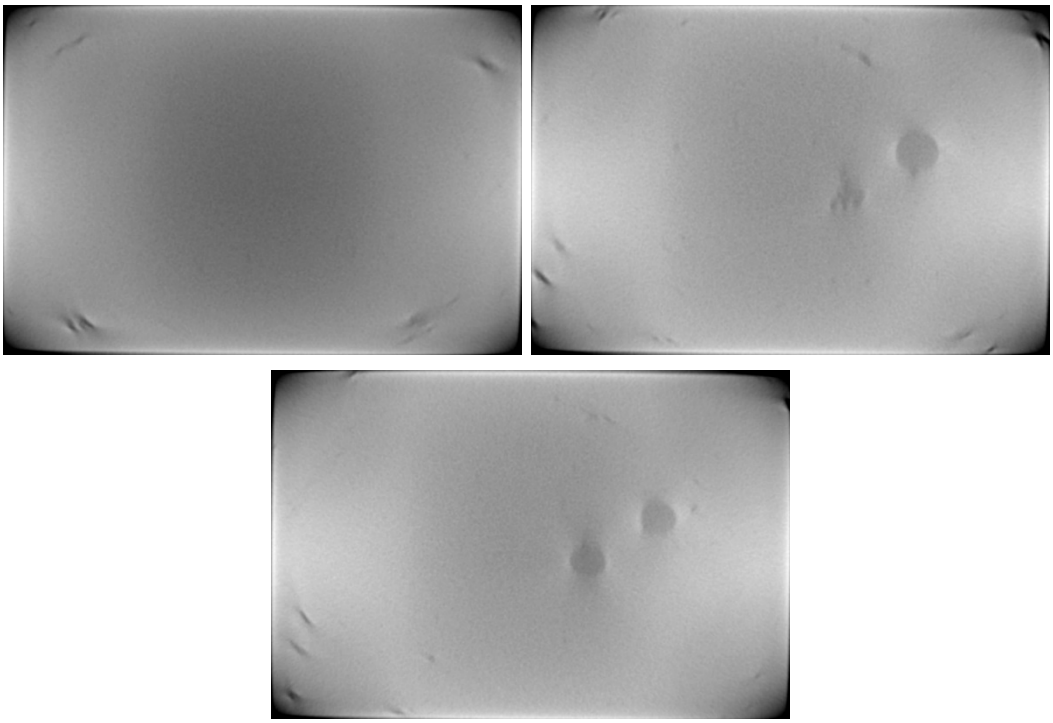

Fig. 52 Top views near the top surface and of the two large voids in the block on the top left, top right, and bottom, respectively

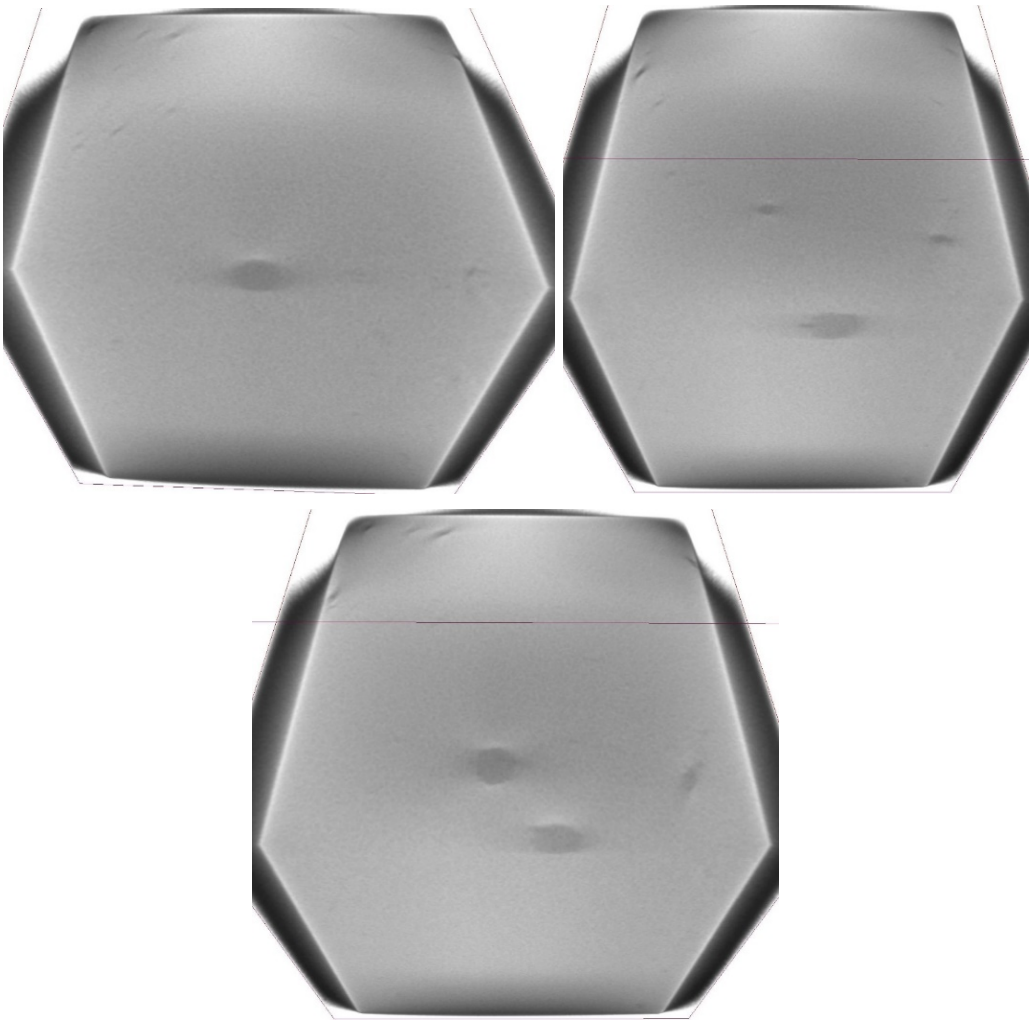

Fig. 53 Double-sectioned 3-D views of each large void individually and both voids together from the front-top perspective in the block on the top left, top right, and bottom, respectively

4.3.4 Block C5

As Figs. 54–58 show, the porosity and voids within block C5 are much like those within the other C blocks, with C5 having a large oval void about 3.0 mm (0.12 inch) × 3.7 mm (0.15 inch) shown in Figs. 55 and 58.

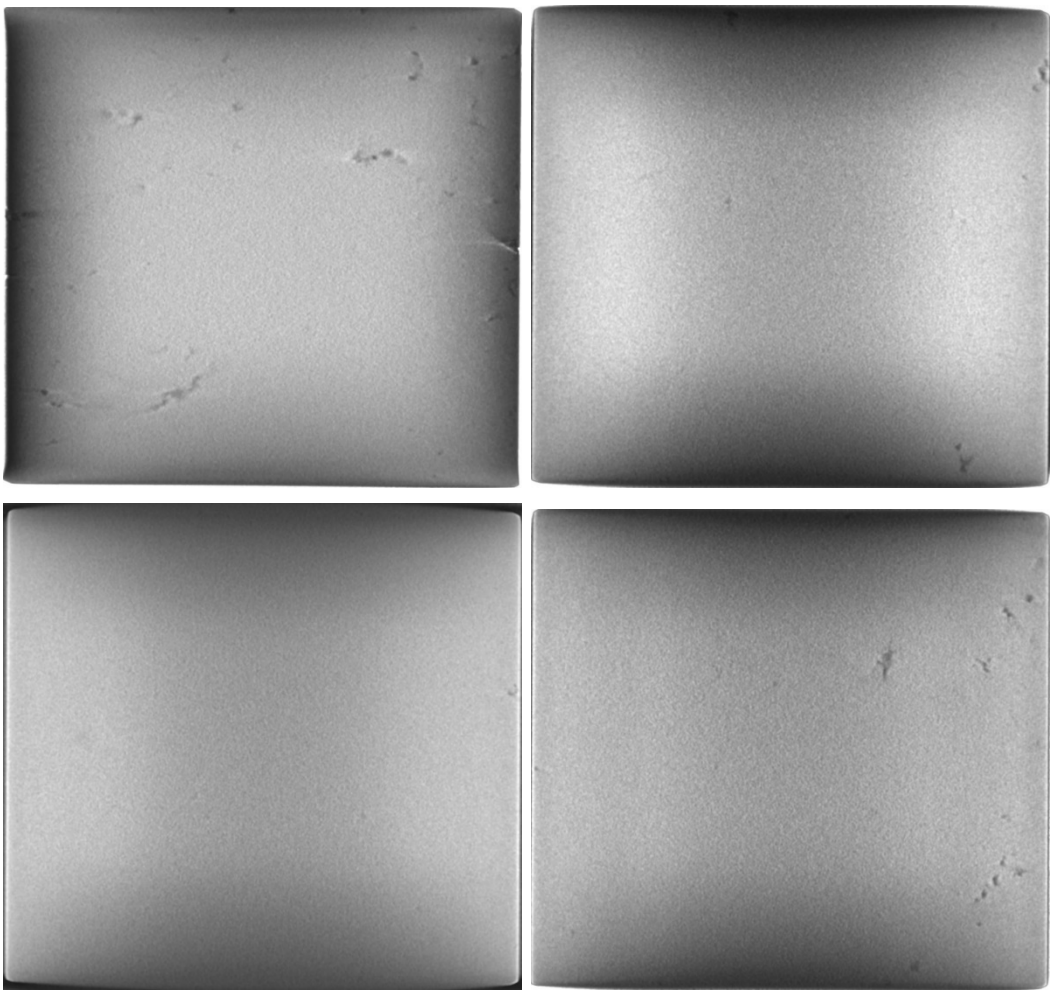

Fig. 54 Front views just inside the front surface and about one-quarter of the way, halfway, and three-quarters of the way through the block on the top left, top right, bottom left, and bottom right, respectively

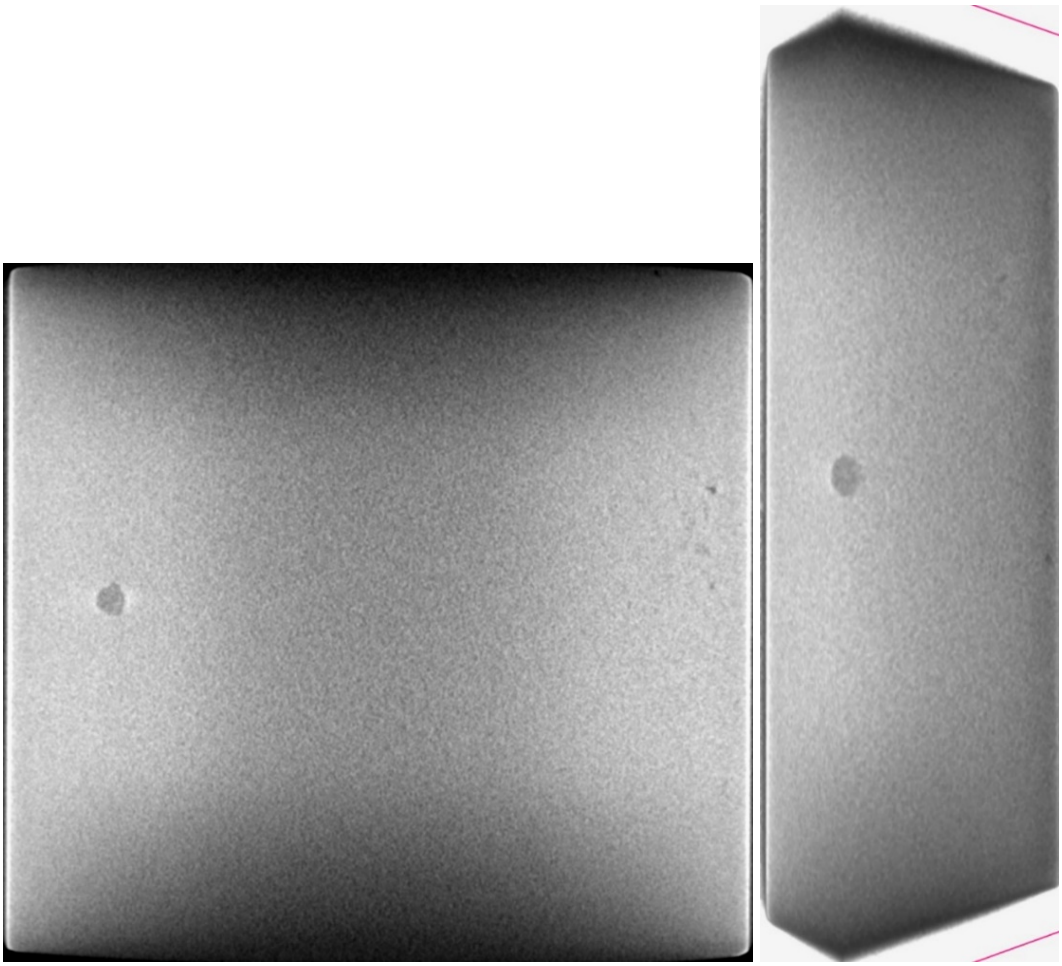

Fig. 55 Front and double-sectioned 3-D views of the large void in the block on the left and right, respectively

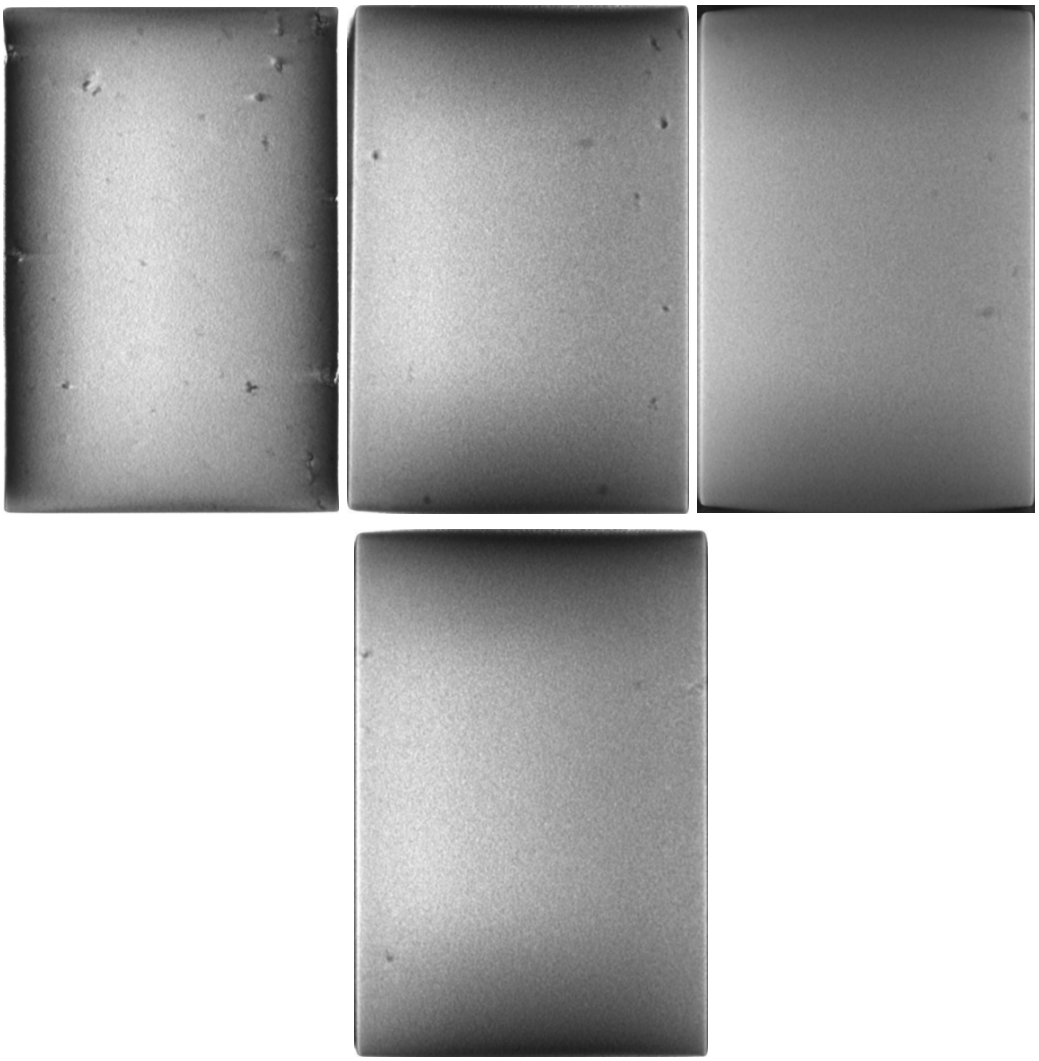

Fig. 56 Side views just inside the right-side surface and about one-quarter of the way, halfway, and three-quarters of the way through the block on the top left, middle, and right, and bottom, respectively

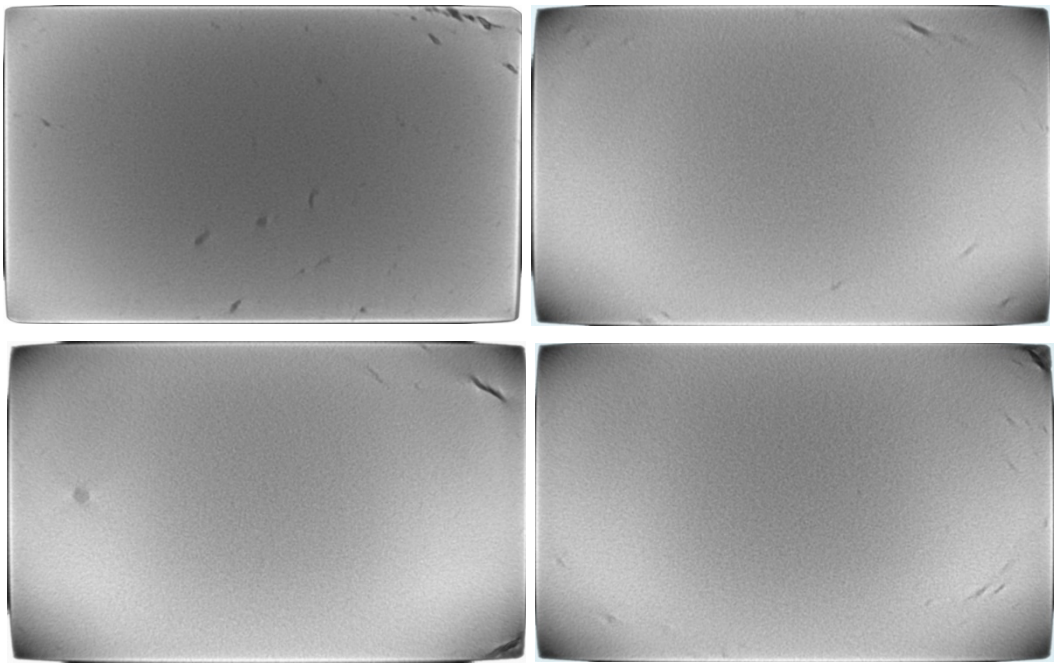

Fig. 57 Top views just inside the top surface and about one-quarter of the way, halfway, and three-quarters of the way through the block on the top left, top right, bottom left, and bottom right, respectively

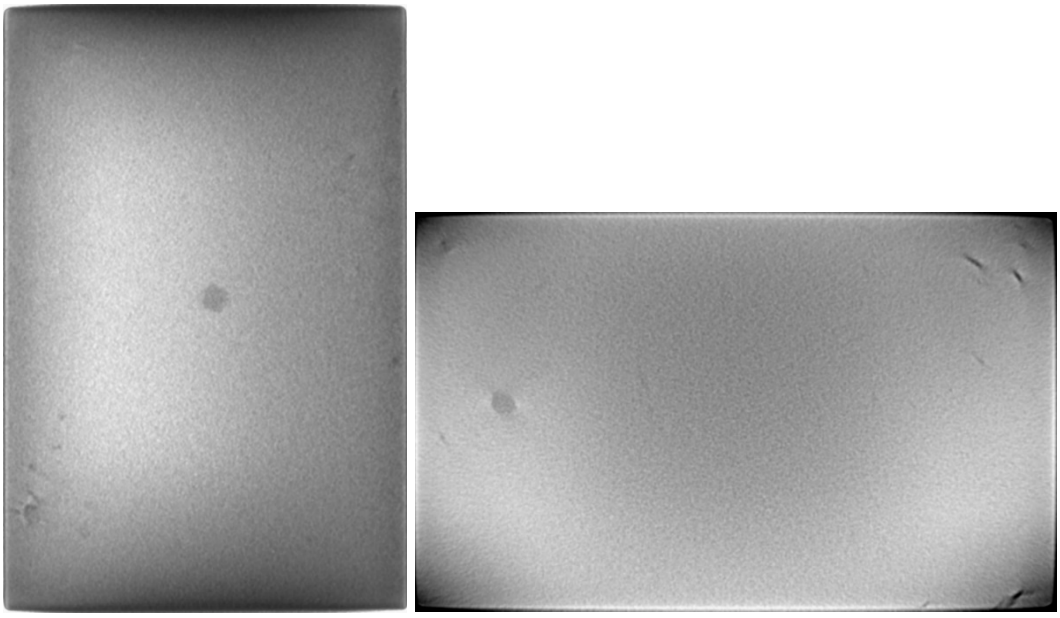

Fig. 58 Side and top view images of the large void in the block on the left and right, respectively

4.3.5 Block C6

As Figs. 59–64 show, the porosity and voids within block C6 are much like those within the other C blocks, with C6 having a medium void about 2.6 mm (0.10 inch) in diameter and a large edge void as shown in Figs. 60 (medium and edge void), 62 (edge void in right image, left side), and 64 (edge void in right image, bottom-right corner).

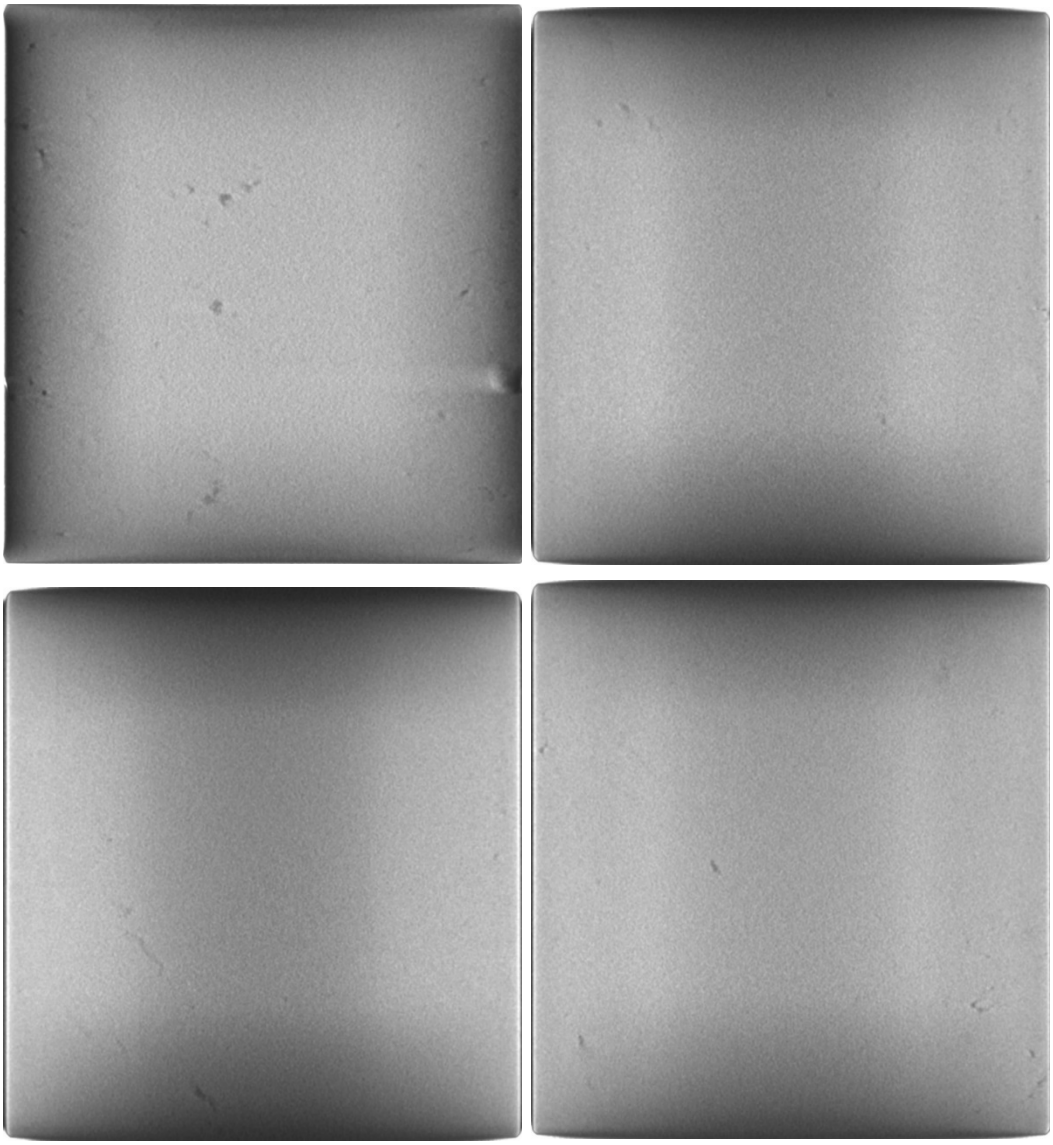

Fig. 59 Front views just inside the front surface and about one-quarter of the way, halfway, and three-quarters of the way through the block on the top left, top right, bottom left, and bottom right, respectively

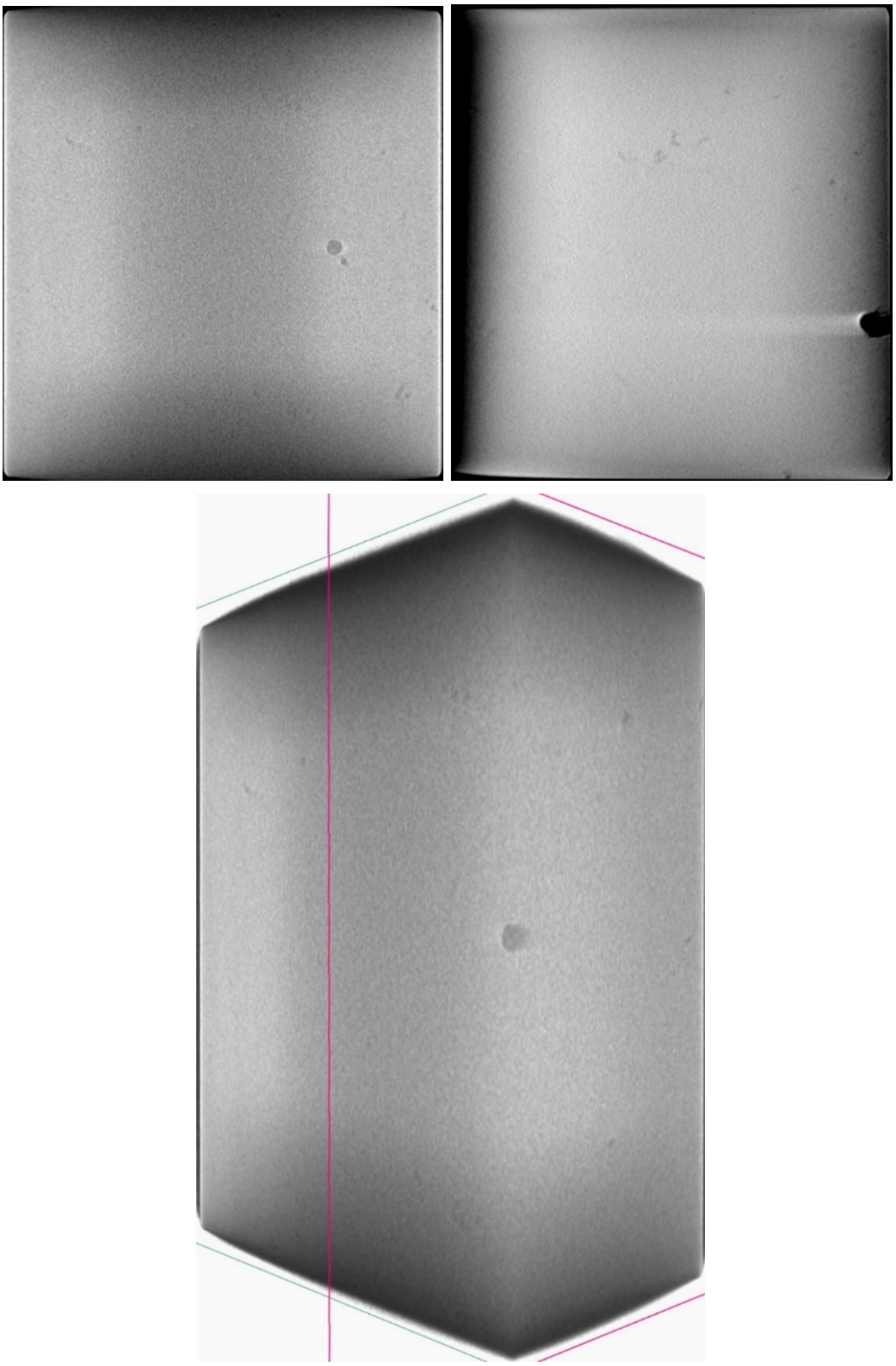

Fig. 60 Front view images of a medium-sized void and an edge void in the block; double-sectioned 3-D view of the medium void in the block on the top left, top right, and bottom, respectively

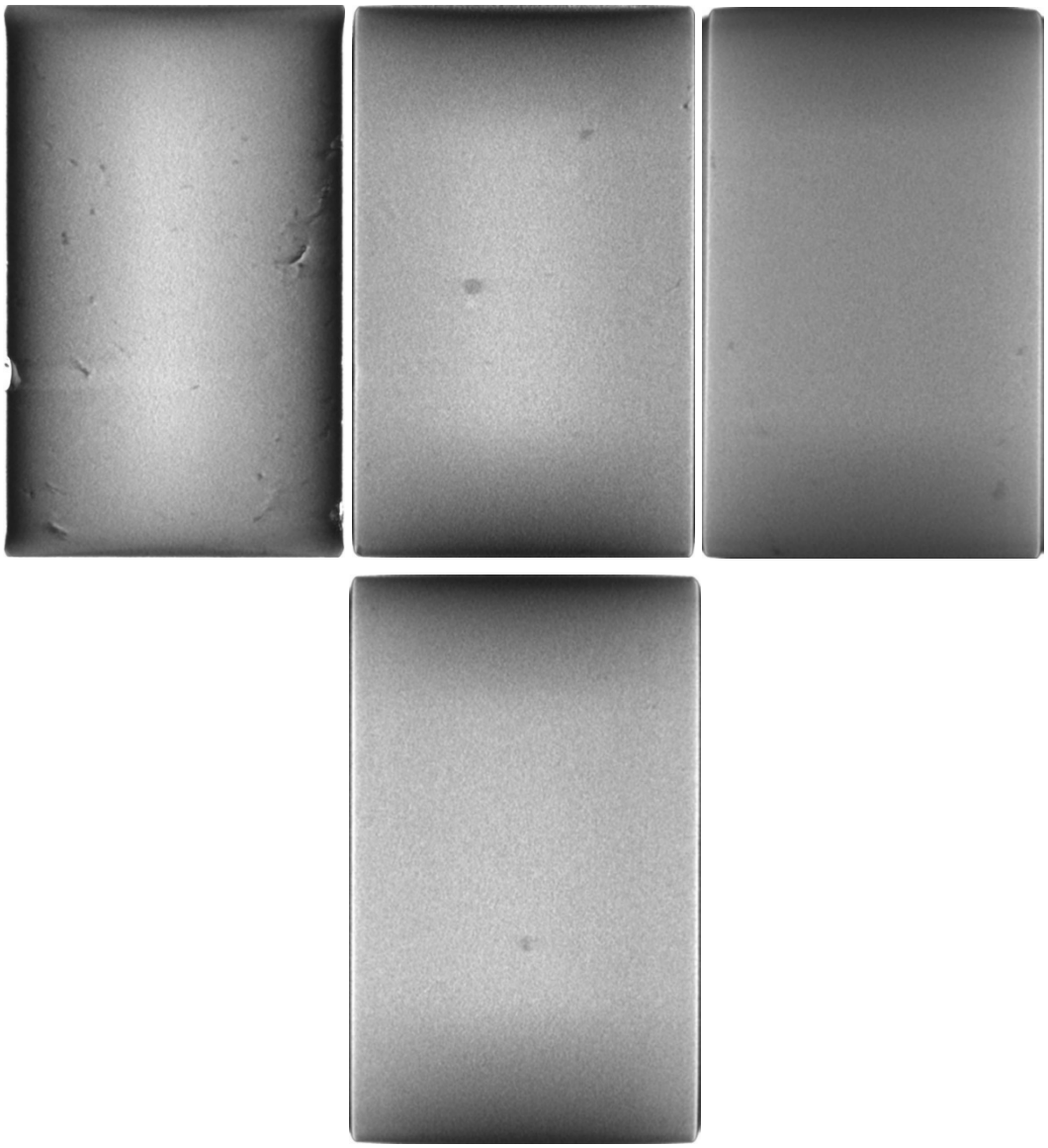

Fig. 61 Side views just inside the right-side surface and about one-quarter of the way, halfway, and three-quarters of the way through the block on the top left, middle, and right, and bottom, respectively

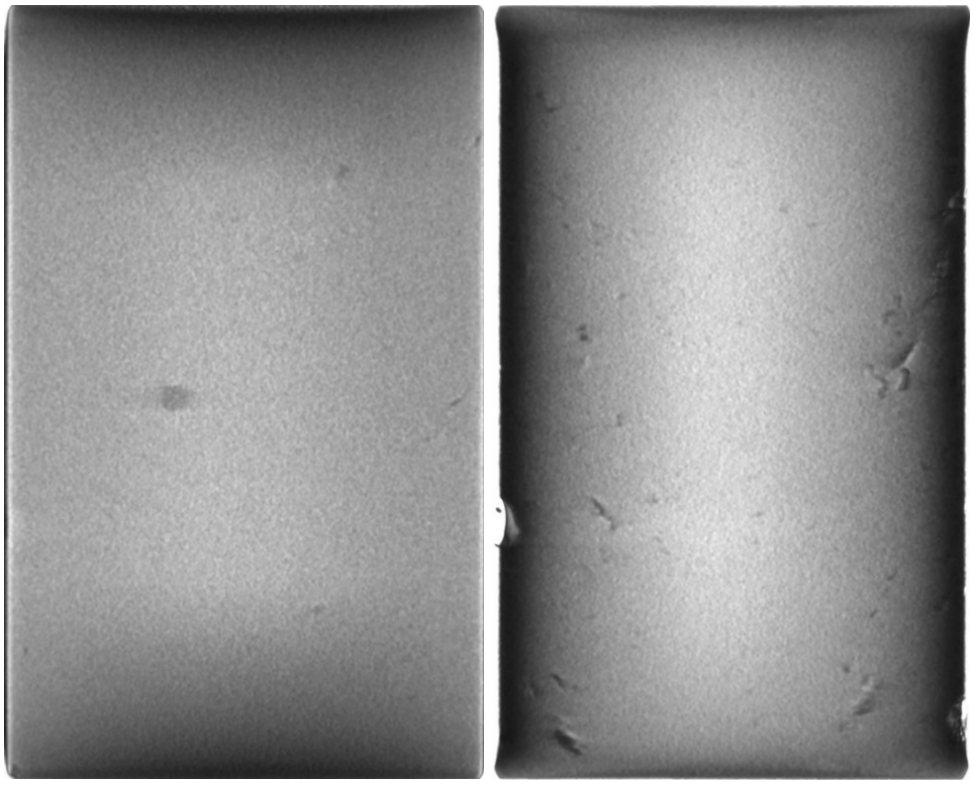

Fig. 62 Side view images of medium-sized void and edge void in the block on the left and right (lower-left side), respectively

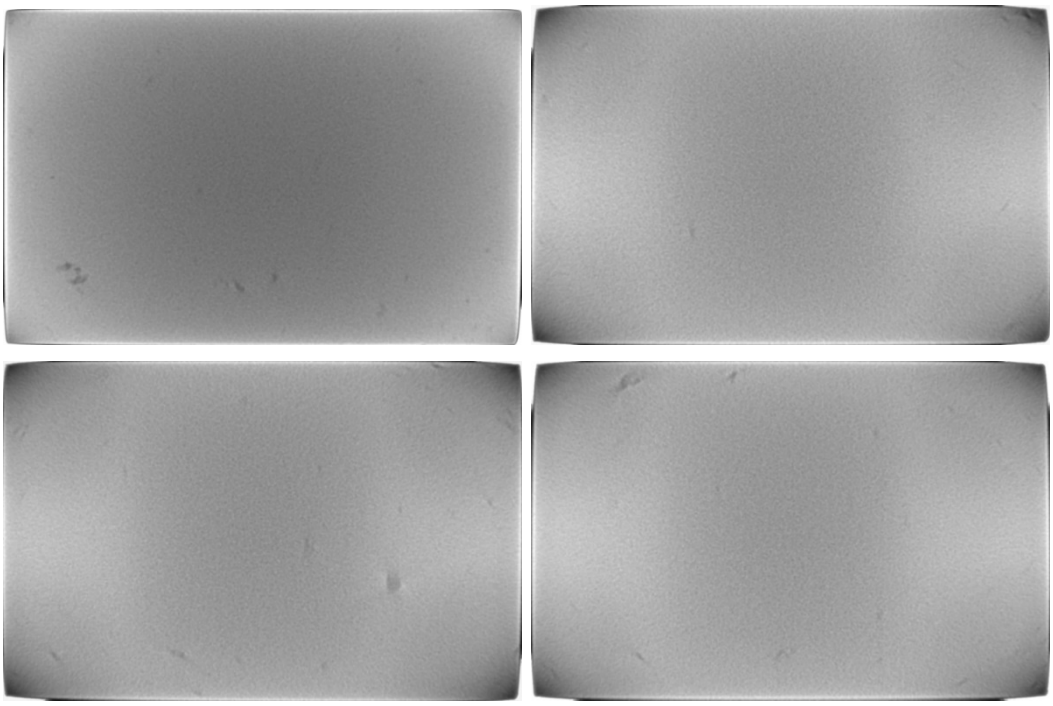

Fig. 63 Top views just inside the top surface and about one-quarter of the way, halfway, and three-quarters of the way through the block on the top left, top right, bottom left, and bottom right, respectively

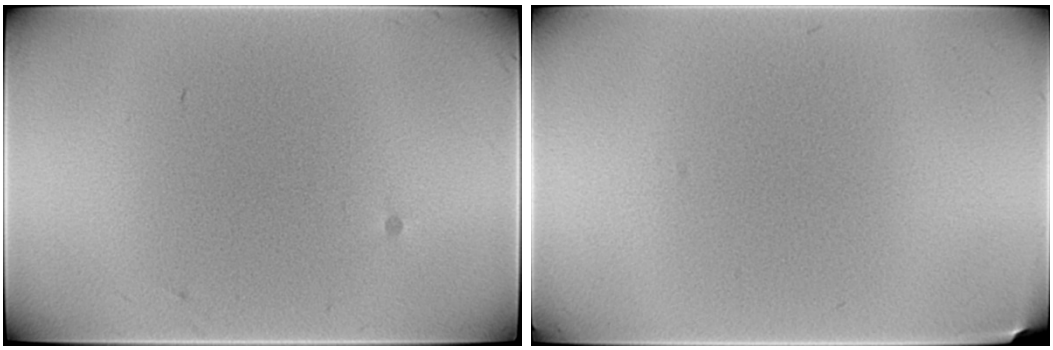

Fig. 64 Top view images of the medium-sized void and edge/corner void (bottom-right corner) in the block on the left and right, respectively

4.3.6 Rolled Block C1

Block C1 was mechanically rolled before the A, B, and C blocks were received for XCT scanning. The block was heated to 1200 °C before rolling. It was held at that temperature for 2 h and then rolled down. Rolling of the block included three passes with a 20% reduction in thickness per pass. Block C1 was oriented with its 50.8-mm (2-inch)-thickness direction vertical at the start of the horizontal rolling process. The process used two rollers rotating in opposite directions with one above and one below the block, resulting in both elongation and thickness reduction. Severe cracking was observed on the second pass, and rolling was halted after the third pass. After rolling was halted, the block was allowed to air cool to ambient temperature.

In Fig. 65, which shows both areal surfaces of the rolled block, it is apparent that both surfaces are cracked, with the surface in the bottom image seemingly more qualitatively cracked than the other. The cracking may be due to a temperature differential during rolling, but this is not certain. The first and second 2-D slice images in Fig. 66 are a few millimeters into the block, close to the more severely cracked surface and about halfway through the block, respectively. The cracking is significantly less severe at the middle thickness location. However, the large cracking or tear in the right-hand side is evident. Both 3-D views in Fig. 67 are sectioned closer to the less-cracked areal surface, with the second view closest to it. The 2-D slice images in Fig. 68 clearly show the overall size and shape of the tear and its extent into the side of the block. The first and second 2-D slice images in Fig. 69 are a few millimeters from the end of the tear and at about the middle of the block, respectively. The images in Fig. 69 are also indicative of the left side of the sectioned surfaces being more severely cracked. Overall, it appears that the areal surfaces and sides of the rolled block are more severely cracked than its interior. One possible contributing factor to this may be that the more asymmetric and crack-like (dendritic) porosity in the unrolled block, assuming C1 had similar

porosity content to the other C blocks, was stretched and compressed by the rolling process, thus being eliminated to a certain extent. Also, this porosity would have been mostly closer to the outside surfaces as opposed to in the middle of the unrolled block. A possible contributing factor to the large tear in the rolled block is the presence of one or more relatively large voids in the originally sectioned unrolled block at the approximate location of the tear. The void or voids could have been about the same size or possibly larger than the relatively large voids in the other C blocks. Elongating essentially in one direction while compressing block C1 during the rolling process may have torn a void or voids open. Continued rolling after forcing a void or voids open may have enlarged the tear.

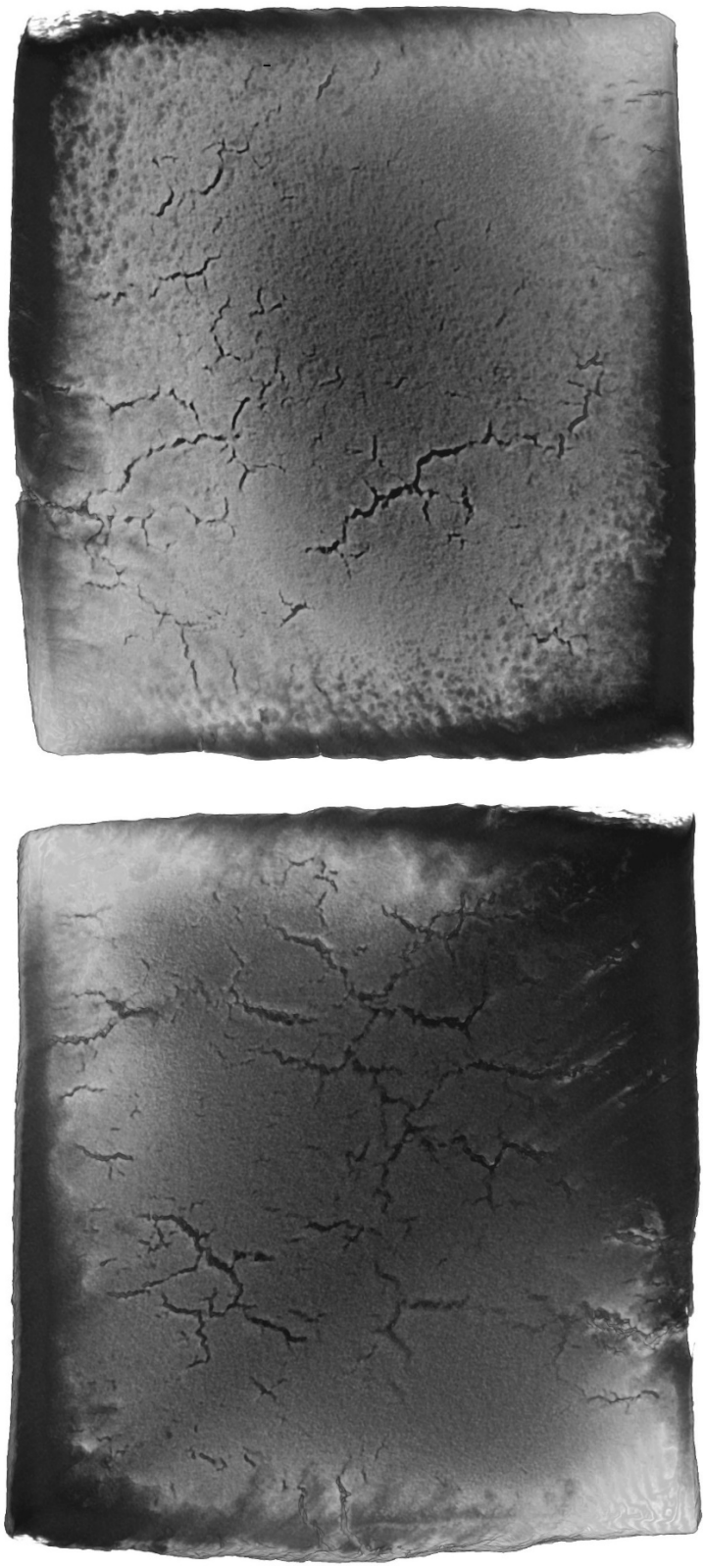

Fig. 65 3-D visualization images of both of the cracked areal surfaces of the rolled block

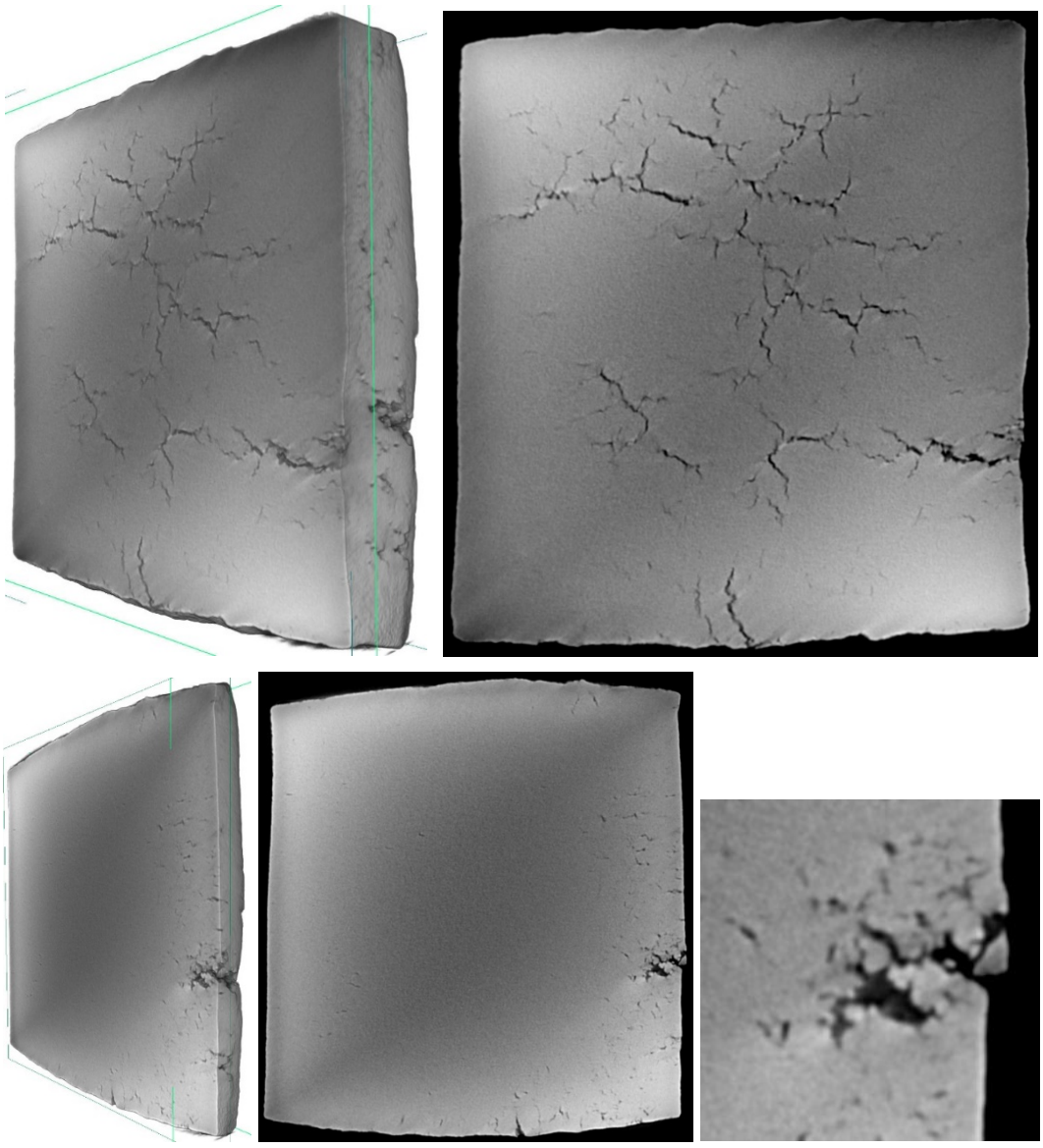

Fig. 66 Set of sectioned 3-D views and corresponding 2-D slice plane images just inside the more severely cracked outer surface and about halfway through in the rolled block (top and bottom left-most two images, respectively); close-up view of the large tear in the right-hand side of the rolled block (bottom-right image)

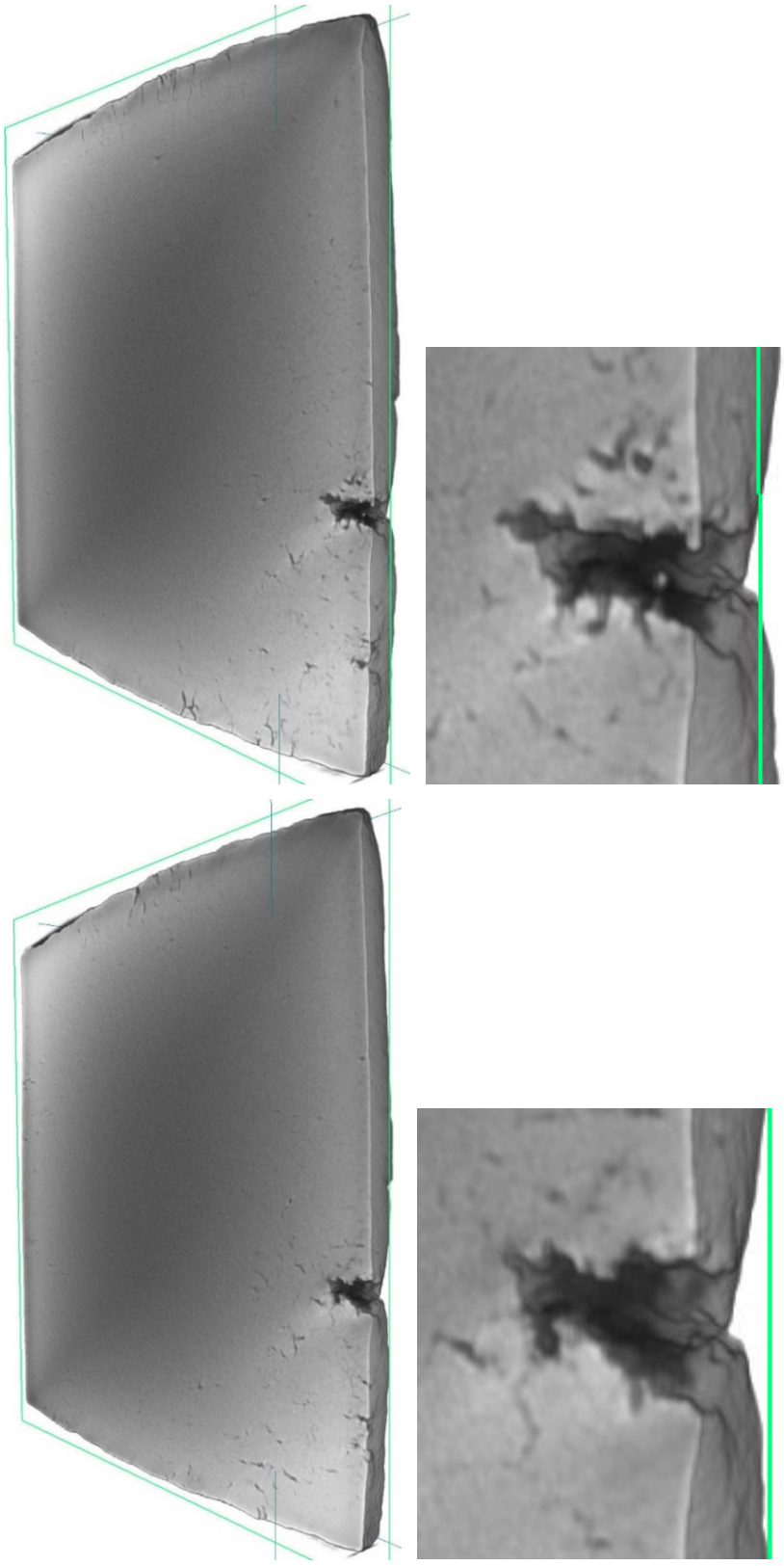

Fig. 67 Two sectioned 3-D views more than halfway through the thickness of the block from the more severely cracked surface and close-up views of the large tear in both

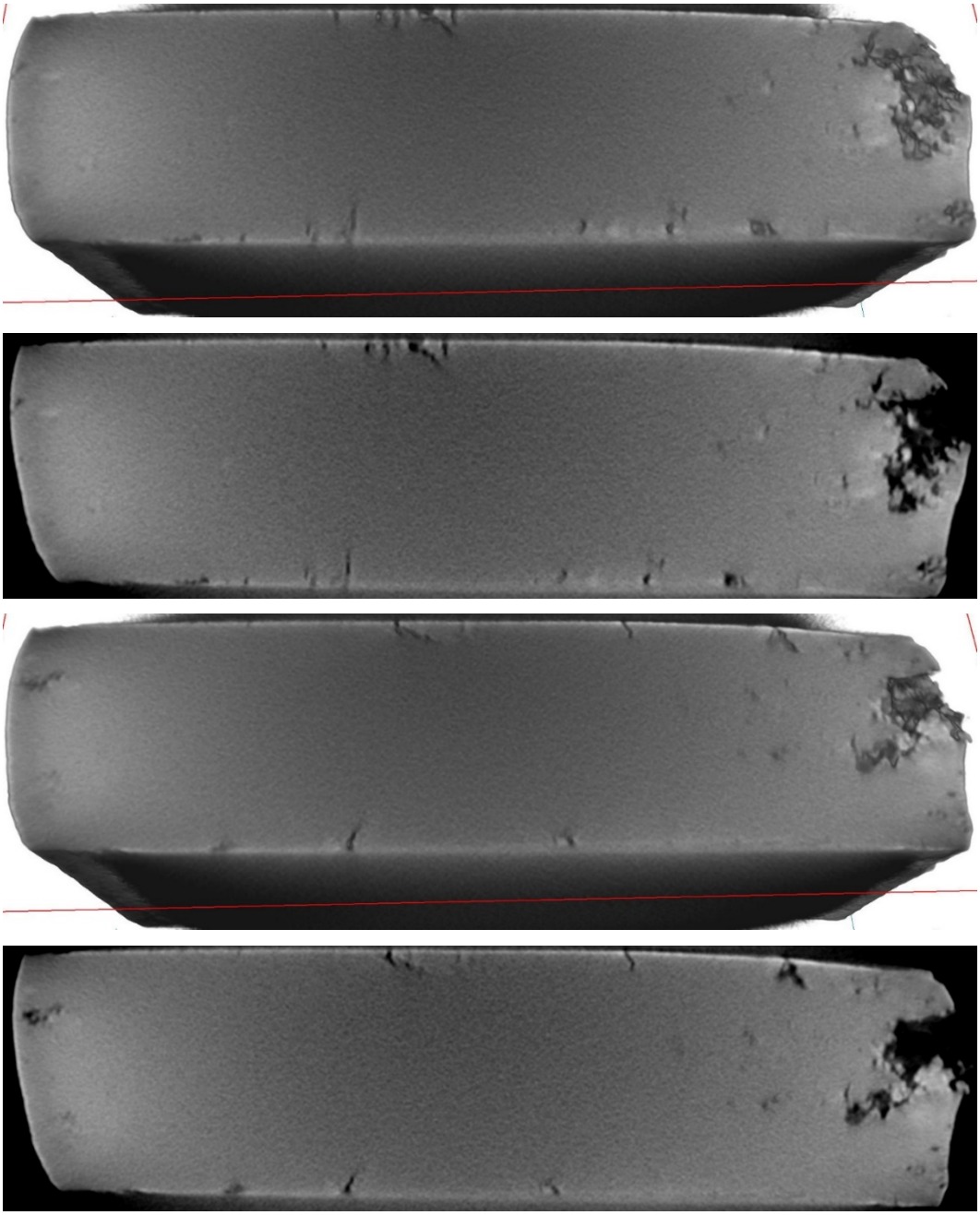

Fig. 68 Set of sectioned 3-D views cutting perpendicular to the areal faces and corresponding 2-D slice plane images with the more severely cracked surface at the bottom of the images

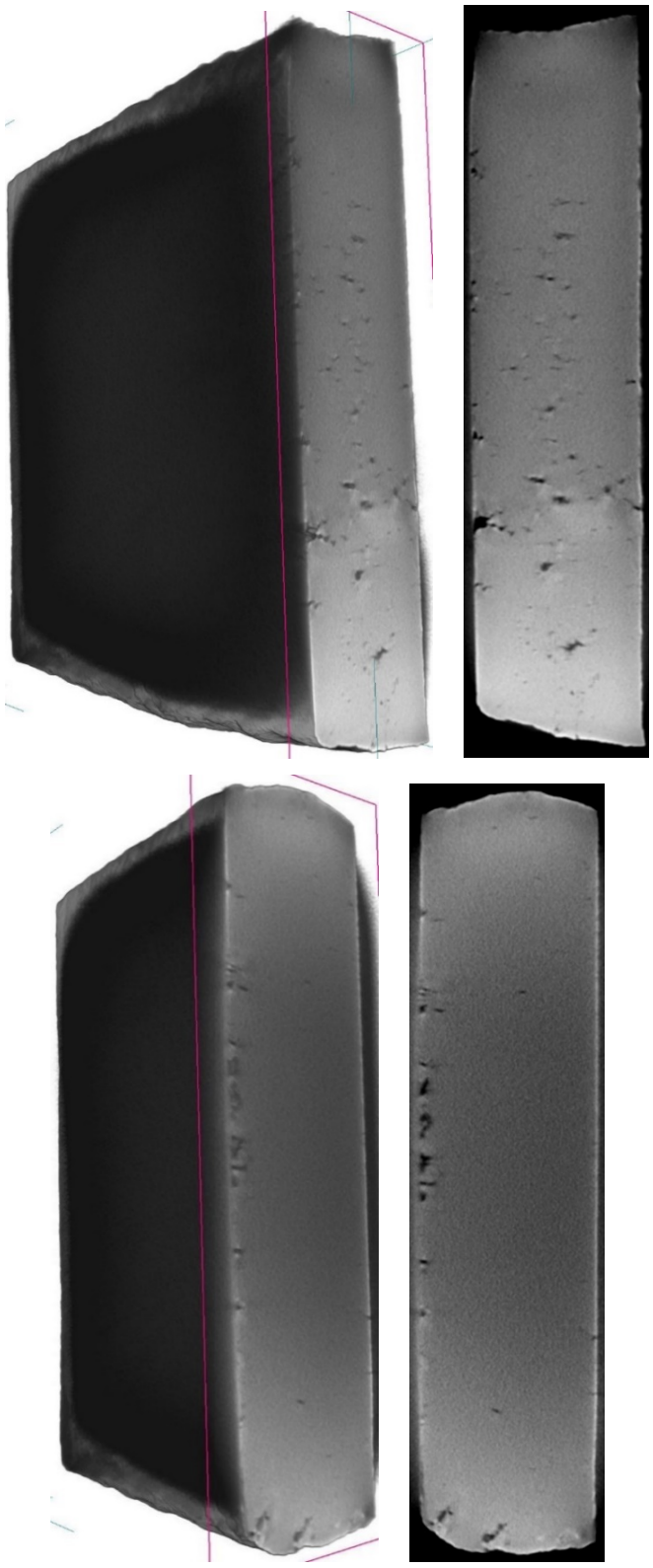

Fig. 69 Set of sectioned 3-D views cutting perpendicular to the areal faces in the orthogonal direction of Fig. 68 and corresponding 2-D slice plane images with the more severely cracked surface on the left

5. Summary and Conclusion

Twelve sectioned FeMnAl steel alloy blocks and one sectioned block that had been mechanically rolled were XCT scanned using frame averaging and oversampling with a 450-kV conventional source in the 400-µm focal spot size mode. Results showed that the A and B block sets sectioned from the perimeter of the cast billet have better overall quality than the C blocks as determined by the number and sizes of detected discontinuities or features. The A blocks have the highest quality, with block A3 having no discernible discontinuities and blocks A2 and A4 having small voids, except for the atypical larger void in A4. The B blocks contain a combination of small voids, short cracks, and missing material along edges or in corners. Blocks B1, B2, and B4 all have detectable small voids. Blocks B2, B3, and B4 all have a small crack, which may have been present in whole or in part before the sectioning process. Blocks B1, B2, and B3 are all missing expanses of material along an edge or at a corner. It is reasonable to consider the missing material of the B blocks to be qualitatively like large voids, since if nominal material was in close proximity to the sectioning locations, it would have remained with the blocks. Block set B is considered to be of lower overall quality than block set A as determined by the number of detectable discontinuity features and their severity. If casting symmetry were to be assumed, the physical features in the A and B block sets would be very, very similar. The relatively short cracks and large expanses of missing material in the B blocks deviate from this assumption. Thus, it is possible that differences in casting properties or conditions, however slight or small, between the two sectioned areas caused the physical differences in the block sets. However, the A and B blocks do not have the extended and asymmetric crack-like features nearer to the outside of the blocks that all the C blocks have.

It is reasonable that the level of porosity and voids in the C block set would be different than in the A or B blocks, since the C blocks were sectioned from the center of the cast billet as opposed to the perimeter. In general, the C blocks contain higher levels of porosity, with one or more relatively large voids near their centers and some voids intersecting edges or corners. The overall nature of the porosity and voids in the C blocks clearly changed from extended and asymmetric, or more crack-like, features nearer to the outside of the blocks to significantly more symmetric, rounded voids in the center regions of the blocks, the edge or corner voids notwithstanding. The A and B blocks do not have similar asymmetric crack-like features, and their internal porosity or voids are generally significantly smaller. Therefore, the overall quality of the C blocks is the worst of the three sets, even though some of the B blocks exhibit missing material along edges or in corners. The nature of the changes in the porosity and voids in the C blocks were likely due to the outside to inside cooling of the material.[9] Block C1 was already

mechanically rolled before it was obtained for XCT scanning. The surface and near-surface regions of block C1 have significantly more cracking and/or porosity than its interior, except for a relatively large fissure or tear in one side of the block. Both of these physical features in the rolled block may be due to the nature of the porosity and voids in the originally sectioned unrolled block, especially if the porosity and voids in the block were similar to those features in the rest of the C blocks. For example, it may be that the more asymmetric and crack-like (dendritic) porosity in the unrolled block located more extensively toward its outside surfaces was stretched and compressed by the rolling process, thus being eliminated to a certain extent, but some porosity and/or cracks significantly closer to the outside surfaces of the rolled block remained as opposed to in the middle interior of it, where there was significantly less asymmetric and crack-like porosity. The fissure or tear in the rolled block could have been affected by the presence of one or more voids in the same approximate location in the originally sectioned unrolled block. The void or voids could have been about the same size or possibly larger than the relatively large voids in the other C blocks. Elongating essentially in one direction while compressing block C1 during the rolling process may have torn a void or voids open. Continued rolling after forcing a void or voids open may have enlarged the tear.

As is evidenced by the thorough characterization of each set of blocks, the XCT technique is a widely applicable and powerful nondestructive inspection modality for evaluation and analysis of geometrical and physical characteristics of materials, especially internal structures and features. This can be the case even in nonoptimal X-ray attenuation and scanning conditions, as was the case in this work scanning and evaluating highly attenuating FeMnAl steel alloy blocks. Effective frame averaging and oversampling the scan space were both applied to mitigate the effects of very high X-ray attenuation and related noise in the resultant XCT data to some extent. Application of effective frame averaging and oversampling the scan space are illustrative of the principle of beginning analysis with the best quality XCT data set reasonably obtainable given the material of interest and overall scan considerations. This sort of approach for maximizing the quality of XCT image data is applicable to any number of nonoptimal high X-ray attenuation, low throughput, and “noisy” (i.e., low S/N) scanning conditions.

6. References

1. ASTM E 1570-95a. Standard practice for computed tomographic (CT) examination. Columbus (OH): American Society for Testing and Materials (ASTM); 1995.

2. Dennis MJ. Industrial computed tomography. In: Ahmad A, Bond LJ, editors. ASM handbook. Cleveland (OH): American Society for Metals (ASM) International; 1989. (Nondestructive evaluation and quality control; vol. 17).

3. Newton TH, Potts DG, editors. Radiology of the skull and brain. St. Louis (MO): The C.V. Mosby Company; 1981. (Technical aspects of computed tomography; vol. 5).

4. Stanley JH. Physical and mathematical basis of CT imaging. Columbus (OH): American Society for Testing and Materials (ASTM); 1986. ASTM CT Standardization Committee (E7.01.07), ASTM Tutorial: Section 3.

5. ASTM E 1441-95a. Standard guide for computed tomography (CT) imaging. Columbus (OH): American Society for Testing and Materials (ASTM); 1995.

6. Muehlhauser B. Optimizing image signal to noise ratio using frame averaging. North Star Imaging Blog; 2015 [accessed 2020 Mar 31]. https://4nsi.com/blog/2015/10/21/optimizing-image-signal-to-noise-ratio-using-frame-averaging/.

7. Shannon CE. Communication in the presence of noise. Proc Inst Radio Eng. 1949;37(1):10–21.

8. Green WH, Cheeseman BA, Field DM, Limmer KR. Advanced X-ray computed tomography of voids and porosity in as-cast FeMnAl steel alloy material. Aberdeen Proving Ground (MD): CCDC Army Research Laboratory (US); 2020 June. Report No.: ARL-TR-8975.

9. Richards V. MET 307 [course syllabus]. [Rolla (MS)]: Missouri University of Science and Technology; 2013. Chapter 4, Risering of castings.

List of Symbols, Abbreviations, and Acronyms

2-D	two-dimensional
3-D	three-dimensional
ARL	US Army Research Laboratory
CCDC	US Army Combat Capabilities Development Command
FeMnAl	iron-manganese-aluminum
S/N	signal-to-noise ratio
XCT	X-ray computed tomography

1 (PDF) DEFENSE TECHNICAL INFORMATION CTR DTIC OCA

1 (PDF) CCDC ARL FCDD RLD CL TECH LIB

8 (PDF) CCDC ARL FCDD RLW M B CHEESEMAN FCDD RLW MB W GREEN J SIETINS T WALTER J SUN FCDD RLW MC C PERGANTIS FCDD RLW MF D FIELD K LIMMER